Supplemental Information Appendix

Biosynthesis of Fosfomycin in Pseudomonads Reveals a New Enzymatic Activity in the Metallohydrolase Superfamily

Max A. Simon[1], Chayanid Ongpipattanakul[2], Satish K. Nair[2,*] and Wilfred A. van der Donk[1,3*]

[1]Department of Bioengineering and Carl R. Woese Institute for Genomic Biology, [2]Department of Biochemistry, [3]Department of Chemistry, Howard Hughes Medical Institute, University of Illinois at Urbana-Champaign, Urbana, IL 61801

Contents

SI Appendix Materials and Methods

All oligonucleotides used in this study were purchased from Integrated DNA Technologies (*SI Appendix* **Table S3**). Reagents used for molecular biology experiments and Luria-Bertani (LB) medium were purchased from New England BioLabs, Thermo Fisher Scientific, MilliporeSigma, or Gold Biotechnology. Plasmid sequencing was performed by ACGT Inc. and constructs are listed in *SI Appendix* **Table S4**. *E. coli* DH5α was used for plasmid maintenance, and *E. coli* BL21(DE3) or Rosetta2 pLysS was used for protein overexpression. Genomic DNA from *P. syringae* PB-5123 was isolated with MoBio UltraClean Microbial DNA Isolation Kit and used for amplification of all genes. gBlocks encoding PsfC homologs were codon-optimized and purchased from Twist Bioscience. Standard molecular biology techniques were employed for cloning of genes using Q5 polymerase. Mutant variants were generated using the QuikChange method with Phusion polymerase.

Expression and Purification of RhiH
The PepM RhiH was purified as described previously (1) for *in vitro* preparation of 2-Pmm.

Expression and Purification of PsfB
E. coli (DE3) Rosetta2pLysS cells harboring the PsfB-encoding plasmid were grown in LB medium supplemented with 34 μg/mL chloramphenicol and 100 μg/mL ampicillin at 37 °C until OD_{600} reached 0.6-0.8. The expression of N-terminally His_6-tagged PsfB was induced by addition of IPTG to 0.25 mM, and the culture was cooled to 18 °C for 16 h. Cells were harvested via centrifugation, washed once with lysis buffer (50 mM HEPES, pH 8.0, 300 mM NaCl, 10 mM imidazole, 2.5% glycerol), and resuspended in the same buffer on ice. Cells were homogenized by two passes through a French Press at 1,000 psi (Thermo Electron Corporation). Lysates were clarified via centrifugation at 30,600 *g* for 1 h. Clarified supernatant was applied to 5 mL of HisPur Ni-NTA resin (Thermo Fisher Scientific) pre-equilibrated with lysis buffer and incubated at 4 °C for 15 min with gentle rotation. The resin was washed twice with lysis buffer, followed by a wash buffer containing 30 mM imidazole. Protein was eluted in the same buffer containing 250 mM imidazole and 10% glycerol. Fractions containing protein identified by a NanoDrop spectrophotometer (Thermo Scientific) were pooled and concentrated in Amicon Ultra centrifugal filters with a 10 kDa molecular weight cut off. The concentrated fractions were desalted using a PD-10 desalting column (GE Life Sciences) pre-equilibrated with storage buffer (50 mM HEPES, pH 8.0, 250 mM NaCl, 10% glycerol) into storage conditions. Eluted protein was snap-frozen in liquid nitrogen and stored at -80 °C.

Expression and Purification of PsfC
Although active during *in vivo* experiments, we were unable to express and purify the original ORF for *psfC* without causing precipitation. A closer analysis of the gene sequence identified a second putative start codon, which offered higher alignment scores with similar sequences during our phylogenetic analysis (underlined in *SI Appendix* **Figure S8**); this second ORF starting at Met14 of the original deposited sequence is referred to here as "PsfC-M2" and was successfully expressed and purified. *E. coli* BL21(DE3) cells harboring the PsfC-M2-encoding plasmid were grown in M9 medium supplemented with the appropriate antibiotic (100 μg/mL ampicillin, 50 μg/mL kanamycin, or 34 μg/mL chloramphenicol), 0.2% glucose, 0.1 mM $CaCl_2$, 1 mM $MgSO_4$, and 0.125 mM $(NH_4)_2Fe(SO_4)_2{\cdot}(H_2O)_6$ at 37 °C until OD_{600} reached 0.6-08. The expression of *N*-terminally His_6-tagged PsfC-M2 was induced by addition of IPTG to 0.25 mM and additional $(NH_4)_2Fe(SO_4)_2{\cdot}(H_2O)_6$ to 0.25 mM. The culture was subsequently cooled to 18 °C and incubated for an additional 16 h. Cells were harvested via centrifugation and washed once with lysis buffer (500 mM NaCl, 50 mM MOPS, pH 7.5, 10 mM imidazole, 10% glycerol). Purifications were conducted both aerobically and anaerobically. Anaerobic purifications and buffer preparation were performed inside a vinyl anaerobic chamber (Coy Laboratory Products, 97% N_2 and 3% H_2). Cells were resuspended in 20 mL of lysis buffer. Cells were homogenized via sonication (30 s on, 1 min off, 20% amplitude, seven cycles). Clarified supernatant was applied to HisPur resin pre-equilibrated with lysis buffer at 4 °C. The

resin was washed twice with lysis buffer, followed by the same buffer with 30 mM imidazole prior to elution with buffer containing 250 mM imidazole and 10% glycerol. Fractions containing protein were pooled, concentrated, and the buffer was exchanged (300 mM NaCl, 50 mM MOPS, pH 7.5) with a 10 kDa Amicon concentrator via centrifugation. Approximately 6 U of thrombin protease (Sigma-Aldrich) per 100 mg His-PsfC was added to the concentrated protein for overnight cleavage at 16 °C. The cleavage progress was determined to be complete by sodium dodecyl sulfate polyacrylamide gel electrophoresis (SDS-PAGE). PsfC-M2 without His_6-tag was purified by passage over a *p*-aminobenzamidine agarose resin (Sigma-Aldrich), followed by application to a HisPur column. The flow-through was collected and concentrated (*vide supra*). Following removal of the His-tag, aerobically purified PsfC-M2 was subjected to size exclusion chromatography (300 mM KCl, 20 mM HEPES, pH 7.5) and subsequently concentrated. The buffer of anaerobically purified PsfC-M2 was exchanged using a PD-10 column preequilibrated with storage buffer (300 mM NaCl, 50 mM MOPS, pH = 7.5, 10% glycerol) or the crystallization buffer (300 mM KCl, 20 mM HEPES, pH 7.5), and the protein was subsequently concentrated. The protein was frozen immediately in liquid nitrogen and stored at -80 °C or used immediately for *in vitro* assays and crystallography.

Semi-synthetic Preparation of 3-OBPn Standard

A solution consisting of enzymatically prepared 2-Pmm or its corresponding isotopologues (*vide supra*) was oxygenated by bubbling O_2 gas through the solution for 30 min. The reaction was initiated by addition of $(NH_4)_2Fe(SO_4)_2{\cdot}(H_2O)_6$ and ascorbic acid to 250 μM and 10 mM, respectively. The reaction proceeded overnight in an open 1.8 mL Eppendorf tube (2-Pmm final concentration approx. 1 mM, 400 μL total volume) and was quenched by addition of EDTA and D_2O to 15 mM and 10%, respectively. Samples were subsequently analyzed by NMR as described below.

NMR Data Processing

Most samples were analyzed on an Agilent NMR instrument operating at 599.70 Hz equipped with a OneNMR Probe for ^{1}H, ^{13}C (150.81 Hz), and ^{31}P (242.77 Hz) measurements. Data were acquired on a spectrometer with gradient/pulse-shaping capabilities and console operating VnmrJ 4.2. Samples were held at 25.0 °C during acquisition. Samples were referenced to internal peaks (^{1}H and ^{13}C), or an external standard of 85% H_3PO_4 for ^{31}P. Spectra were processed using MestReNova (Mestrelab Research) version 12.0.3. A total of 1024 acquisitions were averaged for one-dimensional ^{31}P experiments. For ^{1}H-^{31}P HMBC acquisitions of lysates, 8 scans per T1 increment and 48 increments in the indirect dimension were acquired. ^{1}H-^{13}C HSQCAD spectra were recorded for ^{13}C-enriched samples with 8 scans per T1 increment and 96 increments in the indirect dimension, while ^{1}H-^{13}C gHMBCAD spectra were recorded with 128 increments in the indirect dimension. For enzyme assays of single-turnover conditions, ^{1}H-^{31}P HMBC acquisitions utilized 16 scans per T1 increment and 48 increments in the indirect dimension. Raw FIDs were imported into MestReNova, processed by reduction of T1 noise, and the projection (sum) of the ^{1}H dimension was extracted. This extracted projection was phased, baseline corrected and apodized with a line-broadening function (1 Hz exponential with a first-point scaling factor of 0.50). ^{1}H-dimension doublets corresponding to either 2-Pmm (~1.9 ppm) or 3-OBPn (~2.9 ppm) were integrated for analysis.

A subset of samples (*SI Appendix* **Figure S14**) were analyzed on a 500 MHz Bruker NMR instrument equipped with a CryoProbe. For 1D ^{1}H-decoupled ^{13}C spectra and ^{31}P spectra without ^{1}H-decoupling, 4096 acquisitions were obtained.

Enzymatic Preparation of 2-Pmm

A reaction mixture consisting of 5 mM phosphoenolpyruvate (PEP), 7 mM acetyl-coenzyme A (AcCoA), 1 mM $MgCl_2$, 0.1 mM $MnCl_2$, 50 mM HEPES pH 7.2, 6 μM RhiH, and 26 μM PsfB, was combined at room temperature and allowed to incubate overnight. *In vitro* 2-Pmm production was more robust using the previously characterized RhiH from the rhizocticin B biosynthetic cluster than with PsfA (1) and thus was used for preparation of 2-Pmm. After 12 h, the mixture was centrifuged through a 3 kDa Amicon centrifugal filter to remove proteins and stored at -20 °C until use. The concentration of 2-Pmm was determined via

^{31}P NMR spectroscopy by comparison to remaining PEP in the sample; approximately 30% product formation was observed (1.6 mM 2-Pmm). Isotopologues used for characterization of 3-OBPn were similarly prepared from either commercial 2-^{13}C-PEP, 3-^{13}C-PEP, or synthetic 2-^{13}C-AcCoA. 2-^{13}C-AcCoA was prepared from the corresponding acetic anhydride as described previously (*SI Appendix* **Figure S4-5**) (2).

Multiple-Turnover Assays with PsfC

For anaerobic experiments, enzymatically synthesized 2-Pmm solutions were deoxygenated by sparging with N_2 gas for 30 min and transfer to a vinyl anaerobic chamber (Coy Laboratory Products, 97% N_2 and 3% H_2) to equilibrate overnight. Anaerobically purified PsfC-M2 (500 μM) was reconstituted with 2 equiv. of $(NH_4)_2Fe(SO_4)_2{\cdot}(H_2O)_6$ in 50 mM MOPS pH 7.5 on ice for 30 min. After reconstitution, the assay was initiated by addition of 2-Pmm (1.2 mM final concentration) and ascorbate (10 mM) to a total volume of 400 µL. After 16 h the reaction was quenched by addition of EDTA to 15 mM, D_2O added to 20%, and protein removed using a 10 kDa Amicon centrifugal filter. The flow-through was transferred to an NMR tube, capped, and removed from the anaerobic chamber for NMR analysis (*vide infra*). For aerobic experiments, PsfC-M2 was reconstituted anaerobically as described previously. As a control, an equivalent quantity of bovine serum albumin (BSA) was incubated anaerobically with 2 equiv. of $(NH_4)_2Fe(SO_4)_2{\cdot}(H_2O)_6$ in 50 mM MOPS pH 7.5 on ice for 30 min. Meanwhile a solution of enzymatically synthesized 2-Pmm (1.6 mM) was aerated via sparging with O_2 for 1 h. After anaerobic incubation, enzyme was removed from the anaerobic chamber and the reaction initiated by addition of oxygenated 2-Pmm and ascorbate (10 mM). After incubation at room temperature for 16 h, the assay was quenched as described previously and analyzed by NMR spectroscopy.

Protein Crystallization and Data Collection

Crystals were originally obtained aerobically using sparse matrix screens and PsfC-M2 (i.e. reconstituted with 2 Fe) at a concentration of 15 mg/mL at a 1:1 ratio of condition and protein solution. Initial hits were further optimized using the sitting drop method, at 9 °C (aerobic preparation) and 18 °C (anaerobic preparation). The initial condition that permitted binding only of a single metal contained 0.17-0.20 M sodium malonate, 18-20% PEG 3,350, and bis-tris propane pH 8.5. The precipitant solution that permitted binding of two metals contained 0.17-0.20 M sodium fluoride, and bis-tris propane pH 6.5. Diamond shaped crystals appeared over the course of three days for both conditions. To obtain density for the second metal, crystals were soaked in 10 mM of $(NH_4)_2Fe(SO_4)_2{\cdot}(H_2O)_6$. Crystals were soaked in precipitant solution containing 20% glycerol prior to vitrification in liquid nitrogen. Data were collected at the Advanced Photon Source (APS) at Argonne National Laboratory via the Life Science Collaborative Access Team (LS-CAT) at beamlines 21-ID-D and 21-ID-G. Initial diffraction data were processed using autoPROC (3). Experimental phases for PsfC-M2 were obtained by soaking crystals with condition supplemented with 5 mM triethyl lead acetate for 4 h, and were processed using PHASER as contained in the CCP4 suite (4, 5). The resultant experimental map (phasing power = 1.7; mean figure of merit – 0.33) was of excellent quality allowing for automated building of the initial atomic model using wARP (6). The structure was further refined using REFMAC5 (7), and was manually built in COOT (8). The near complete model was then used to carry out refinement against data collected on crystals of Psf13 soaked with Fe^{2+} under anaerobic conditions. Anomalous maps were calculated using data collected near the iron absorption edge (1.73 Å).

Phylogenetic Tree of PHP Domain

A PSI-BLAST search with PsfC as the bait sequence was conducted under standard parameters. The search was stopped after one iteration, as the PsfC sequence was lost in further iterations. The resulting closest neighbors were dereplicated and aligned using MAFFT with G-INS-i parameters, and a simulated maximum-likelihood phylogenetic analysis was performed using FastTree (9, 10). Sequences obtained through PSI-BLAST were also submitted to the program RODEO to determine their local genetic context and assign their context-based function, if any (11).

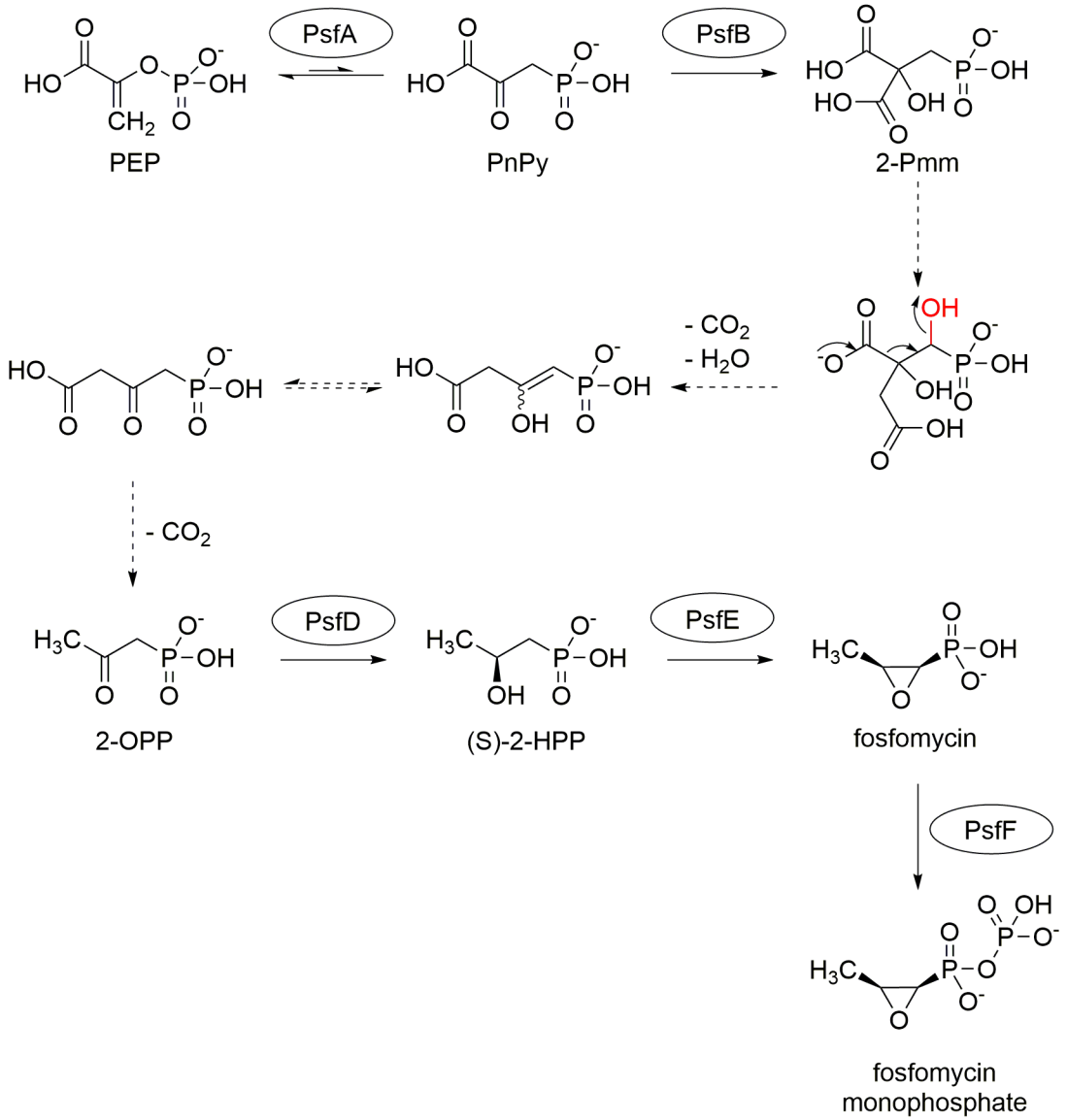

Figure S1. Previously proposed biosynthesis of fosfomycin in Pseudomonas (12). A) Following chemical logic and common occurrence in phosphonate biosynthetic routes, hydroxylation at Cα in 2-Pmm could afford α-hydroxy-2-Pmm. This intermediate could subsequently eliminate water concomitant with decarboxylation to afford an enolic species. This enol can tautomerize to form the β-keto product, 3-OBPn, which can decarboxylate either spontaneously or enzyme-catalyzed to 2-OPP, a previously characterized on-pathway intermediate. The PsfF reaction is believed to be a resistance mechanism (13-15).

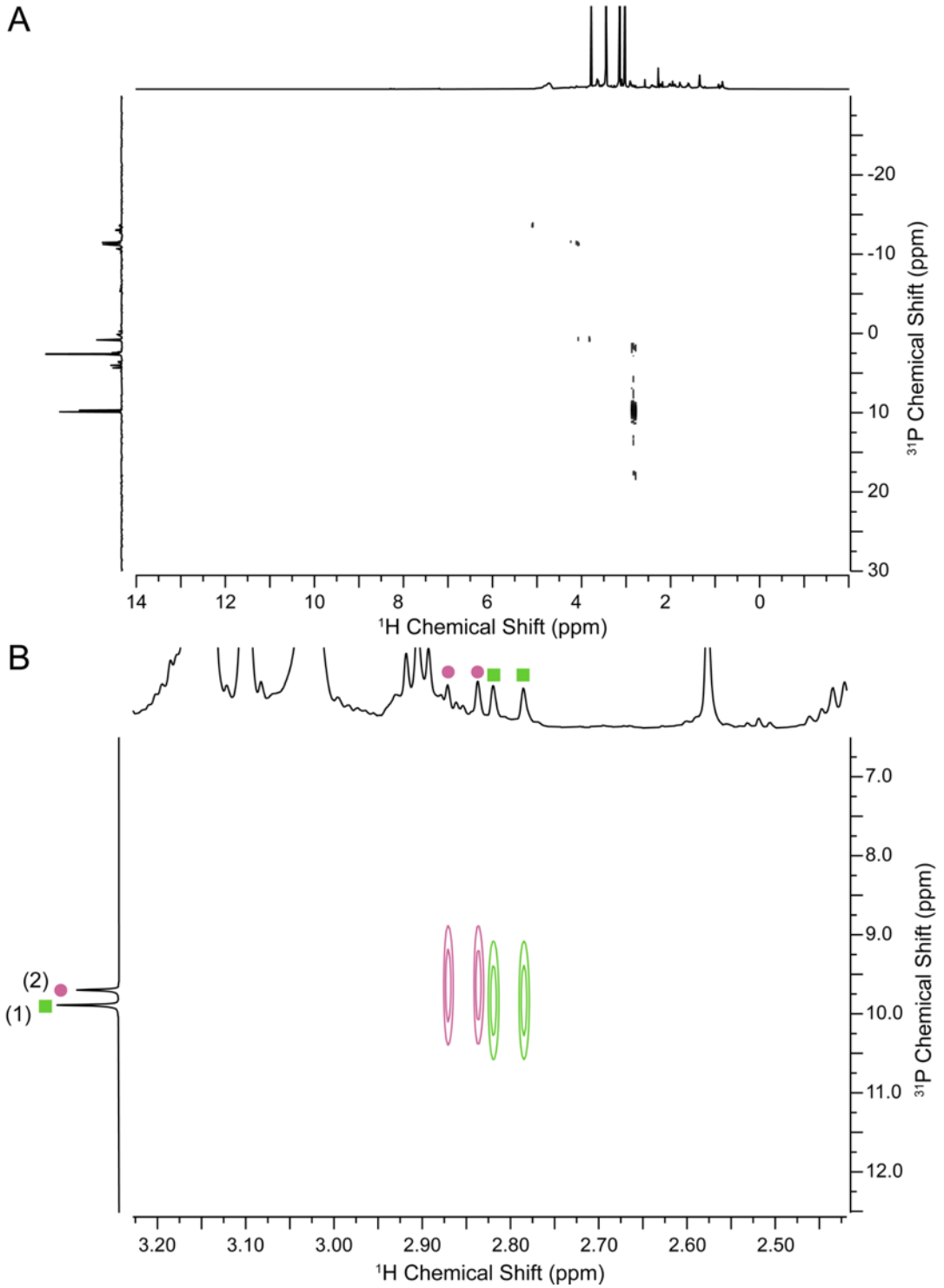

Figure S2. ^{1}H-^{31}P HMBC NMR spectrum of *psfABC*-expressing *E. coli* cell lysate. (A) Full spectrum indicates large cross-resonances at ~10 ppm (^{31}P) and ~3 ppm (^{1}H). (B) Zoom in on this set of resonances shows that each phosphorus signal is coupled to unique protons, each presented as a doublet due to the ½ spin of the ^{31}P nucleus. The cross peaks can be directly observed in the 1D ^{1}H spectra traced above. Cross peaks correlated to compound **1** are represented in green, those to compound **2** are represented in pink.

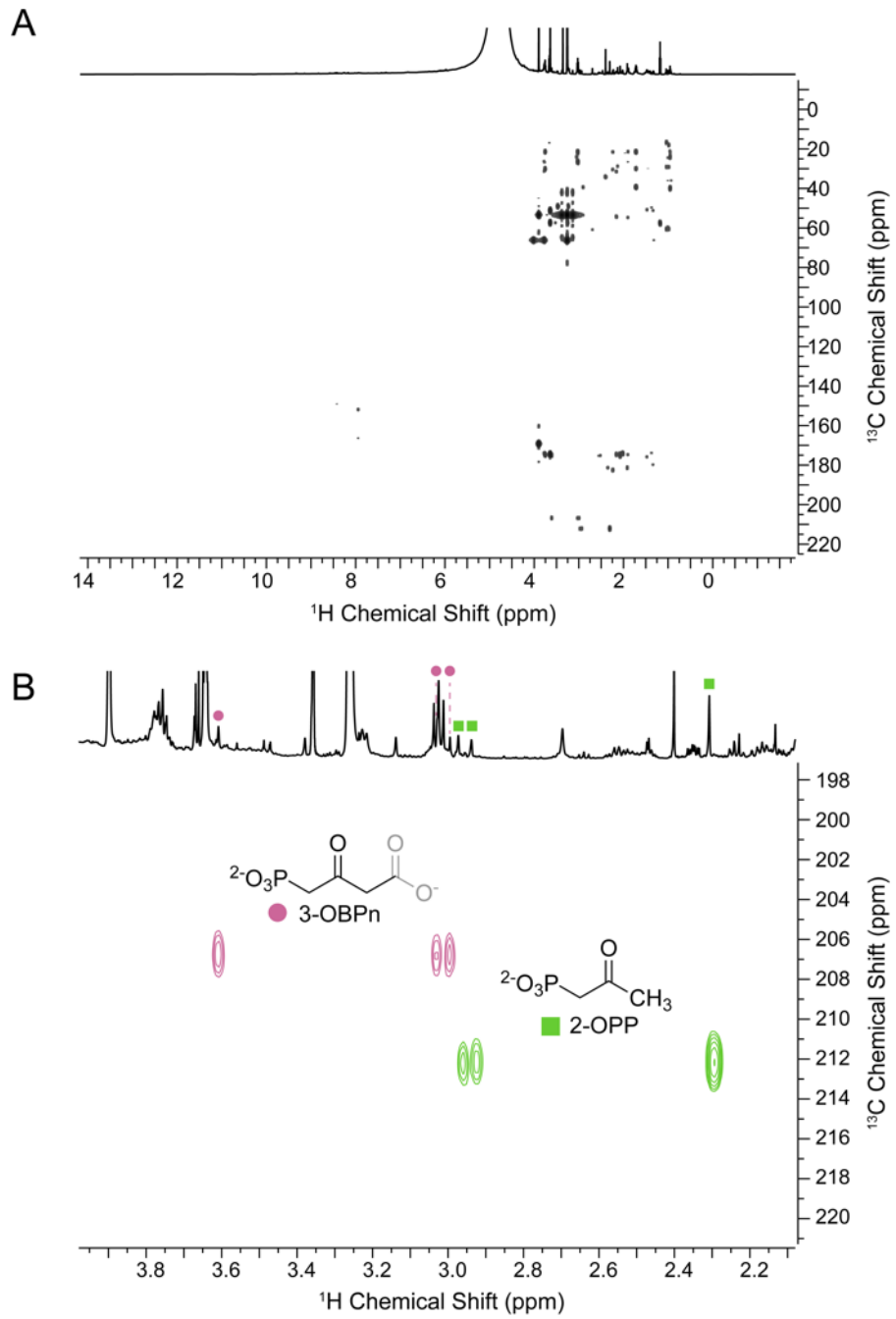

Figure S3. ^{1}H-^{13}C gHMBCAD NMR spectrum of cell lysate of *E. coli* expressing *psfABC*. (A) Full spectrum indicates only two sets of ^{13}C cross peaks correlate to the protons identified in Figure S2. (B) Zoom in on this set of resonances shows that these protons correlate by ^{2}J coupling to carbonyl carbons at approximately 206-212 ppm. The protons associated with compound **1** in green at 2.95 ppm are coupled to the same carbonyl resonance as an additional set of protons centered at 2.30 ppm. When integrated, these two signals have a ratio of 2:3, providing support for their assignment to the methylene and methyl groups of 2-OPP, respectively. The protons at 3.05 ppm associated with compound **2**, shown in pink, are correlated with a ^{1}H resonance at 3.6 ppm in addition to a carbonyl carbon at ~207 ppm. Thus, the structure drawn in black is supported by these data but the part of 3-OBPn drawn in light grey is hypothetical. However, the assignment of the product **2** to 3-OBPn is also supported by spiking with authentic standards (see main text).

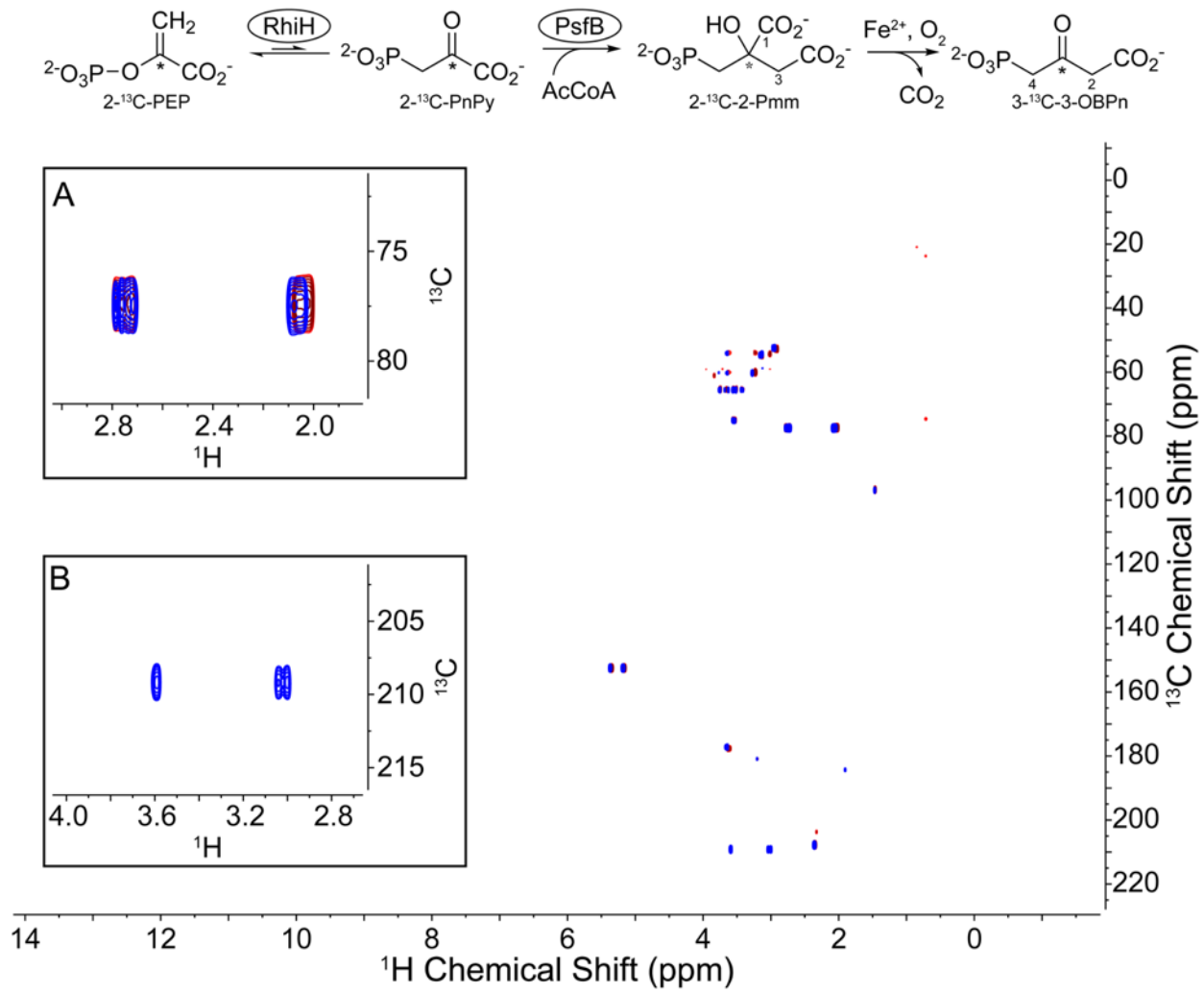

Figure S4. ^{1}H-^{13}C gHMBCAD spectrum of 3-OBPn. 2-^{13}C-2-Pmm generated enzymatically from 2-^{13}C-PEP was reacted with ferrous ammonium sulfate and molecular oxygen to form 3-^{13}C-3-OBPn *in vitro*. The asterisk (*) represents the ^{13}C-label in the molecule. Overlaid ^{1}H-^{13}C gHMBCAD data for 2-^{13}C-2-Pmm and its oxidative decarboxylation product are shown. Cross peaks shown in red correspond to unreacted 2-Pmm, where blue peaks correspond to peaks in the sample after reaction. Inset A corresponds to both methylene protons of 2-Pmm in the starting material and in the sample after reaction (unreacted starting material). Inset B shows the formation of a new product with resonances at ~3.0 ppm and ~3.6 ppm that couple to the labeled carbon that has a chemical shift near 210 ppm. The cross-peak doublet at ~3.0 ppm for the C4 protons is due to the ½ spin of the ^{31}P nucleus. The singlet at ~3.6 ppm corresponds to the C2 methylene protons that also couple to the ^{13}C labeled carbon with a chemical shift near 210 ppm.

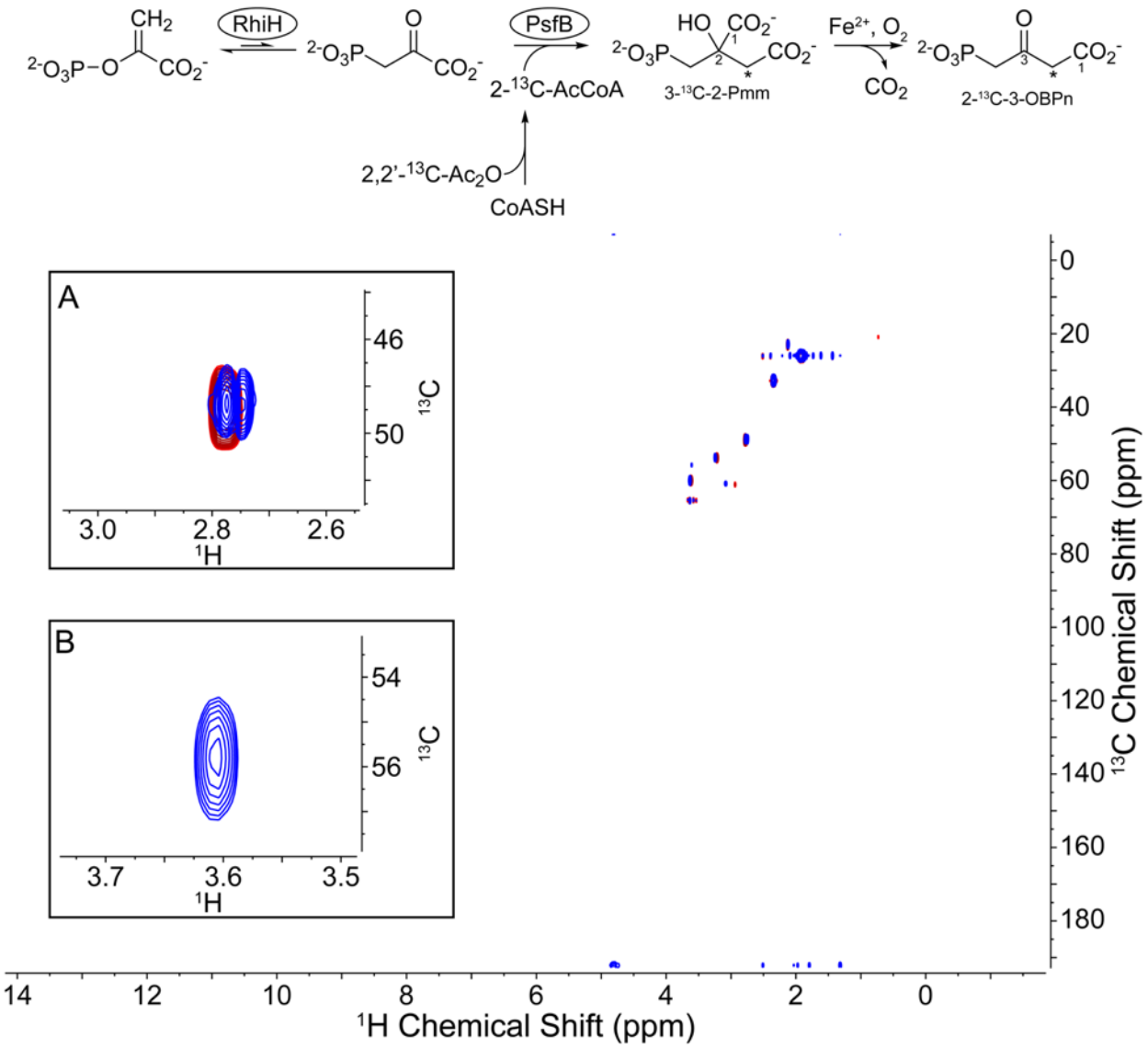

Figure S5. ^{1}H-^{13}C HSQCAD spectrum of 3-OBPn. 3-^{13}C-labeled 2-Pmm generated enzymatically using 2-^{13}C-AcCoA was reacted with ferrous ammonium sulfate to form 2-^{13}C-3-OBPn *in vitro*. The asterisk (*) represents the ^{13}C-label in the molecule. Overlaid ^{1}H-^{13}C HSQCAD data for 3-^{13}C-2-Pmm and its decarboxylation product are shown. Cross peaks shown in red correspond to unreacted 3-^{13}C-2-Pmm, and peaks in blue correspond to3-OBPn product. Inset A shows 2-Pmm ^{1}H signal coupled to the labeled carbon in starting material (red) and in unreacted starting material after the iron-catalyzed reaction (blue). Inset B shows the crosspeak of the ^{13}C-labeled C2 methylene carbon of the product 2-^{13}C-3-OBPn with the same protons at 3.6 ppm observed in *SI Appendix* **Figures S3-4**.

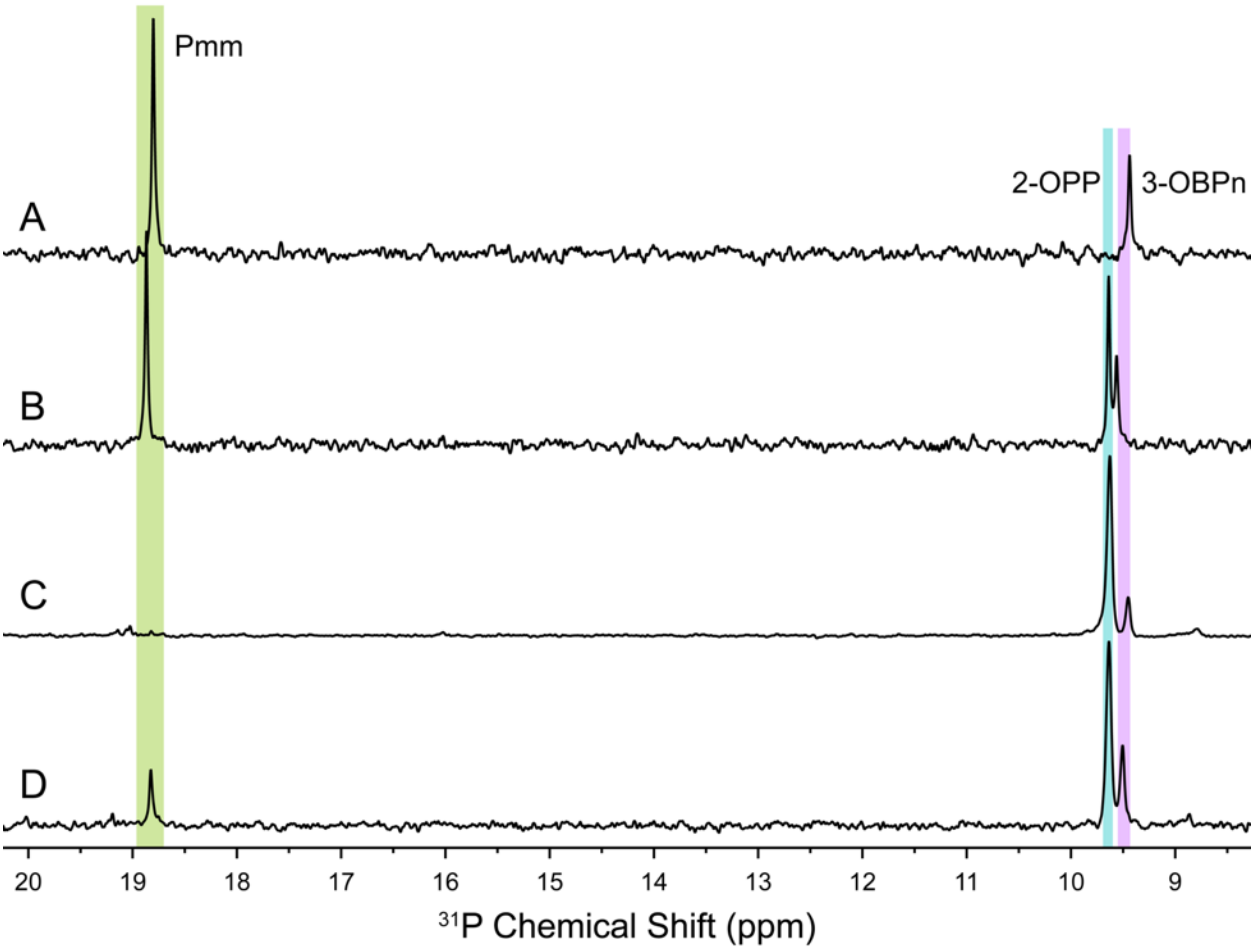

Figure S6. ^{31}P NMR spectra of synthetic 2-OPP and semi-synthetic 3-OBPn standards. These standards were spiked into lysates of *E. coli* cells that expressed *psfABC*. (A) Product of the Fe-catalyzed non-enzymatic decarboxylation of Pmm. (B) Addition of authentic 2-OPP to (A) demonstrates that the product in A has a chemical shift that is upfield from 2-OPP. (C) Lysate of *E. coli* cells that co-expressed PsfABC. (D) Addition of the sample from panel A to the sample of panel C results in an increase in the intensity of the upfield peak (from 11.6 to 28.4% compared to 2-OPP abundance). ^{31}P chemical shifts are sensitive to pH near their pK_a resulting in small shifts from experiment to experiment.

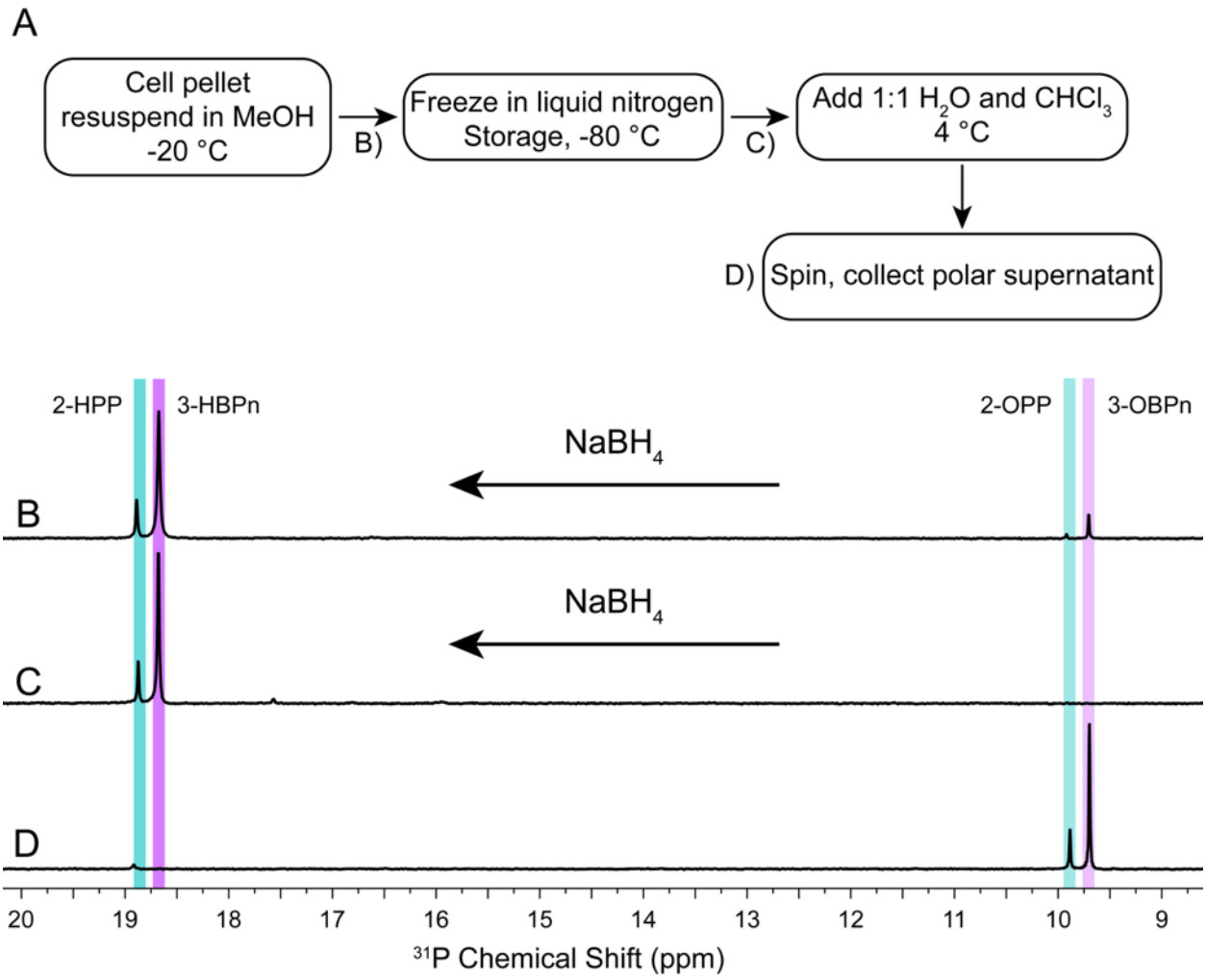

Figure S7. ^{31}P NMR spectra for chemical reduction of lysates of *psfABC* expressing *E. coli* cells. (A) General scheme for work-up illustrated for preparing cell lysates. $NaBH_4$ was added as indicated at points "B" and "C." (B) Cell lysate was treated with $NaBH_4$ upon methanol extract of washed cell pellets. Near complete reduction of 2-OPP and 3-OBPn is observed. (C) Methanol extracts were thawed from storage at -80 °C to 4 °C, and $NaBH_4$ was subsequently added alongside cold water and chloroform (4 °C). Complete reduction is observed with similar product ratios between 2-OPP/2-HPP and 3-OBPn/3-HBPn as in (B) and in panel D. (D) Lysate from non-treated cells that produced 2-OPP and 3-OBPn. The small peak at ~19 ppm corresponds to 2-Pmm in this sample. Ratio of 2-OPP:3-OBPn is consistent between untreated and treated cells.


WP_018249103.1
WP_054877098.1
KUO58778.1
WP_088104464.1
WP_091234269.1
PsPsfC
Ps106PsfC
BsPsfC
GbPsfC

Figure S8. Sequence alignment of selected PsfC-like proteins. Accession numbers in purple are associated with proteins encoded in putative phosphonate BGCs based on gene context, and whose function was verified *in vivo* in this study. Accession numbers highlighted in orange are associated with BGCs that do not have a known function. Residues were highlighted based on four consensus types. Residues highlighted in green are invariant residues conserved amongst all sequences, independent of their genomic context and implied function. In purple are residues that are conserved amongst proteins encoded within a phosphonate biosynthesis context, but not conserved in the other protein sequences. In orange are variable residues within the phosphonate-associated sequences but that are conserved in the sequences from non-phosphonate BGCs. Highlighted in pink are positions that are conserved in phosphonate-related and non-phosphonate BGCs but are distinguished from each other (e.g. residue 26 is a conserved lysine for non-phosphonate proteins, but a leucine for phosphonate-associated proteins). Residues targeted for mutagenesis that impact the activity of PsfC are shown with an asterisk (*) above the corresponding position. Residues that did not completely impede function when mutated to alanine are shown with a dot (•) above the residue. The methionine start site used for purifying *Ps*PsfC is underlined.

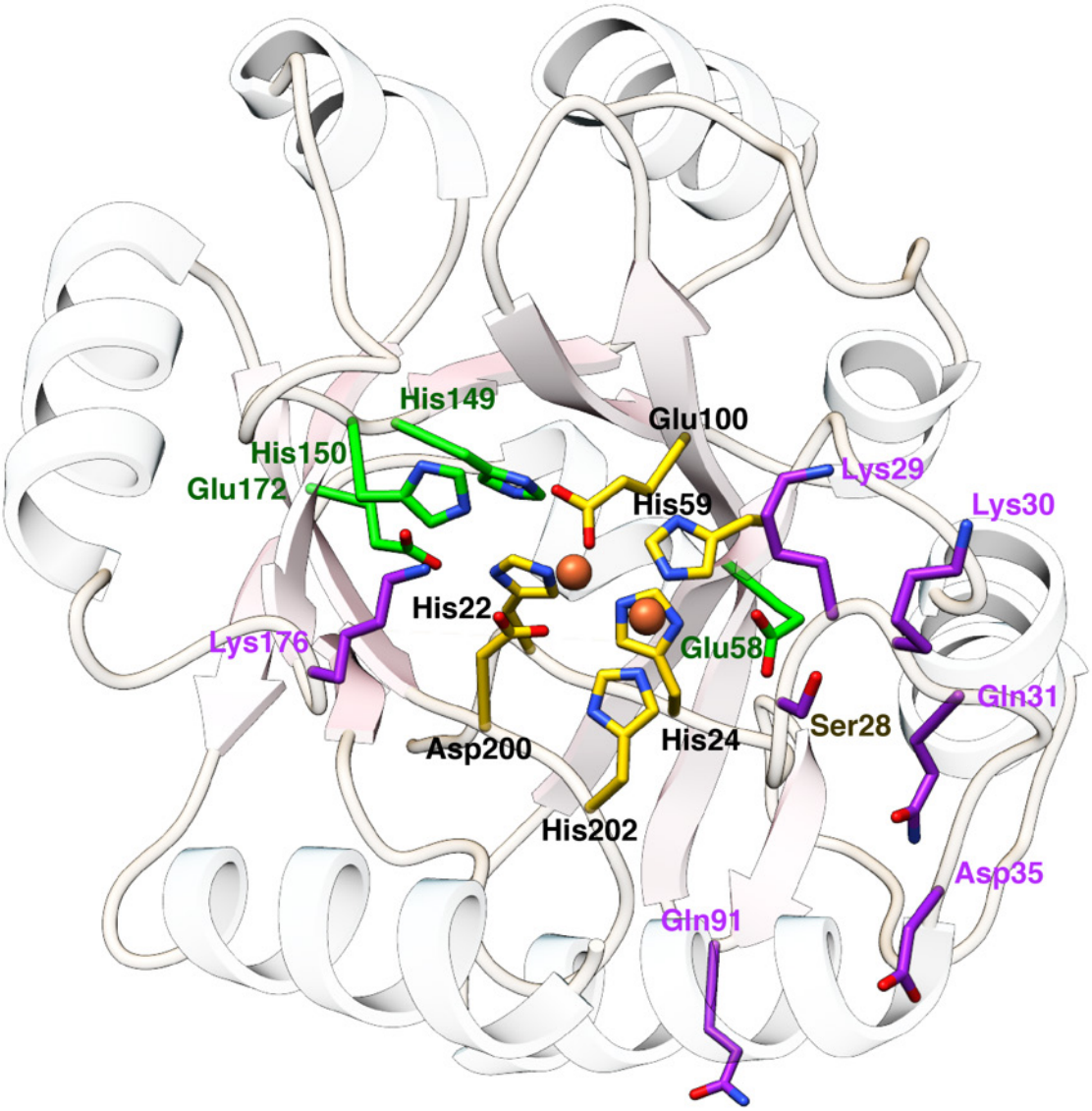

Figure S9. Structure of PsfC showing the residues that were substituted by alanine to assess their importance for catalysis. Residues shown in gold abolished activity. Residues shown in purple had a negligible effect on activity. Residues shown in green aberrated function of the enzyme but are not expected to be metal ligands.

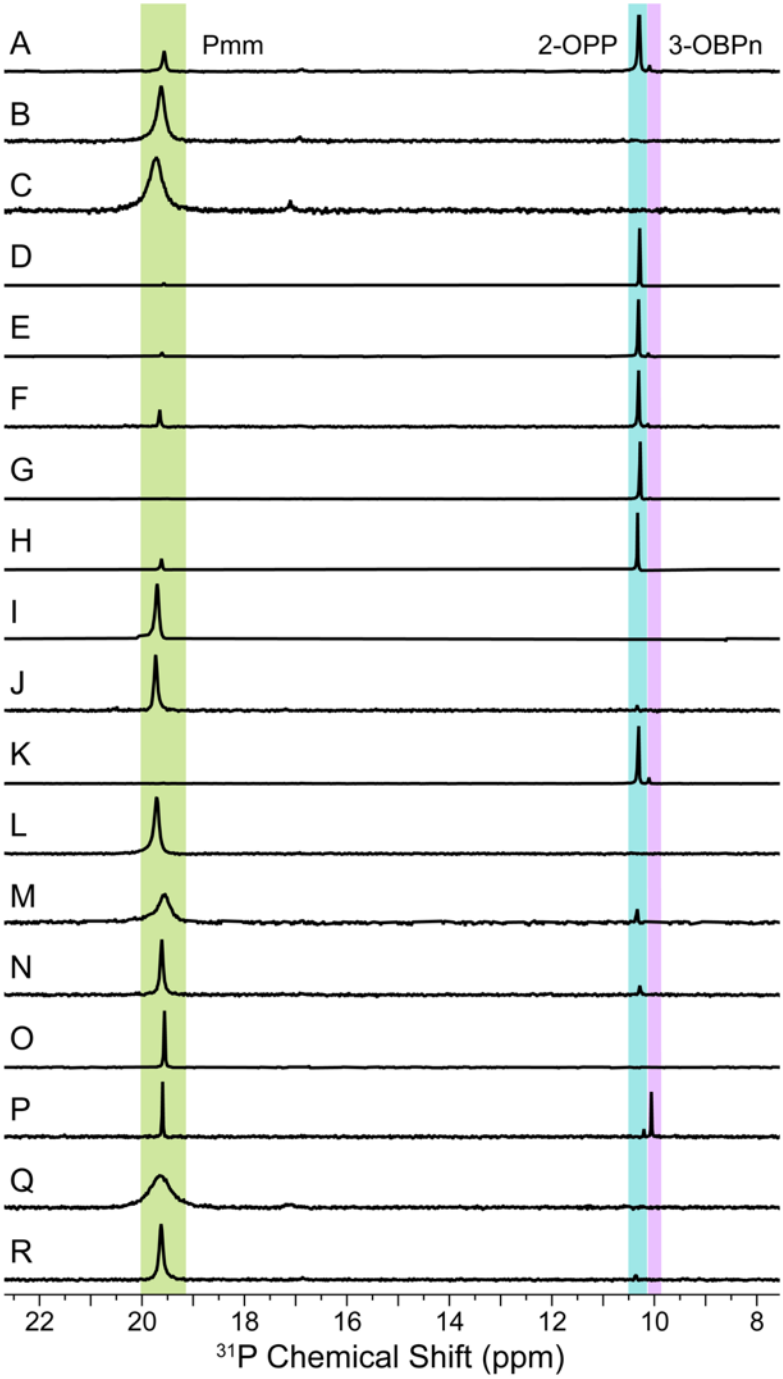

Figure S10. Activity of PsfC variants when co-expressed with PsfAB in *E. coli* determined by ^{31}P NMR spectroscopy. A) Wild-type (WT) *psfC* co-expressed with *psfAB*, and (B-R) *psfC* variants: B) His22Ala, C) His24Ala, D) Ser28Ala, E) Lys29Ala, F) Lys30Ala, G) Gln31Ala, H) Asp35Ala, I) Glu58Ala, J) His59Ala, K) Gln91Ala, L) Glu100Ala, M) His149Ala, N) His150Ala, O) Glu172Ala, P) Lys176Ala, Q) Asp200Ala, and R) His202Ala. ^{31}P chemical shifts are sensitive to pH near their pK_a resulting in small shifts from experiment to experiment. Compound identity was confirmed by ^{1}H-^{31}P HMBC NMR. All experiments involve work-up conditions that convert most 3-OBPn to 2-OPP.

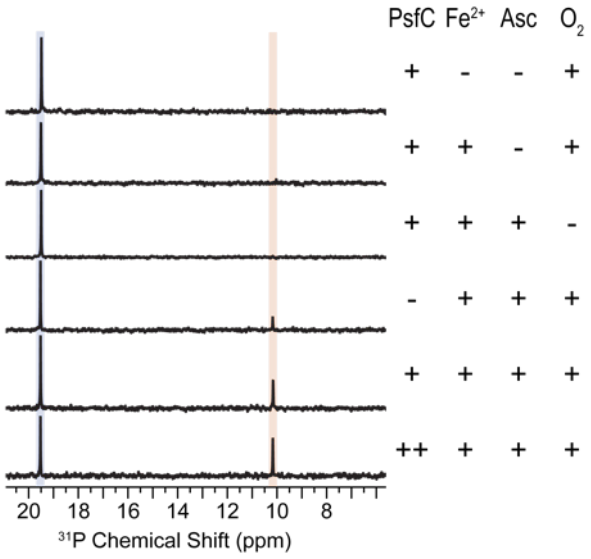

Figure S11. ^{31}P NMR spectra of *in vitro* assays with PsfC. Depicted is the phosphonate region of the ^{31}P NMR spectra; peaks corresponding to 2-Pmm (blue) and 3-OBPn (orange) are indicated. Assays were performed with 2-Pmm (1.2 mM final concentration) and PsfC-M2 (100 μM where indicated, "+") with or without added components determined to be necessary for multiple turnovers – O_2, Fe^{2+}, and ascorbate ("Asc"). Increase of PsfC-M2 concentration from 100 to 150 μM increased product formation ("++").

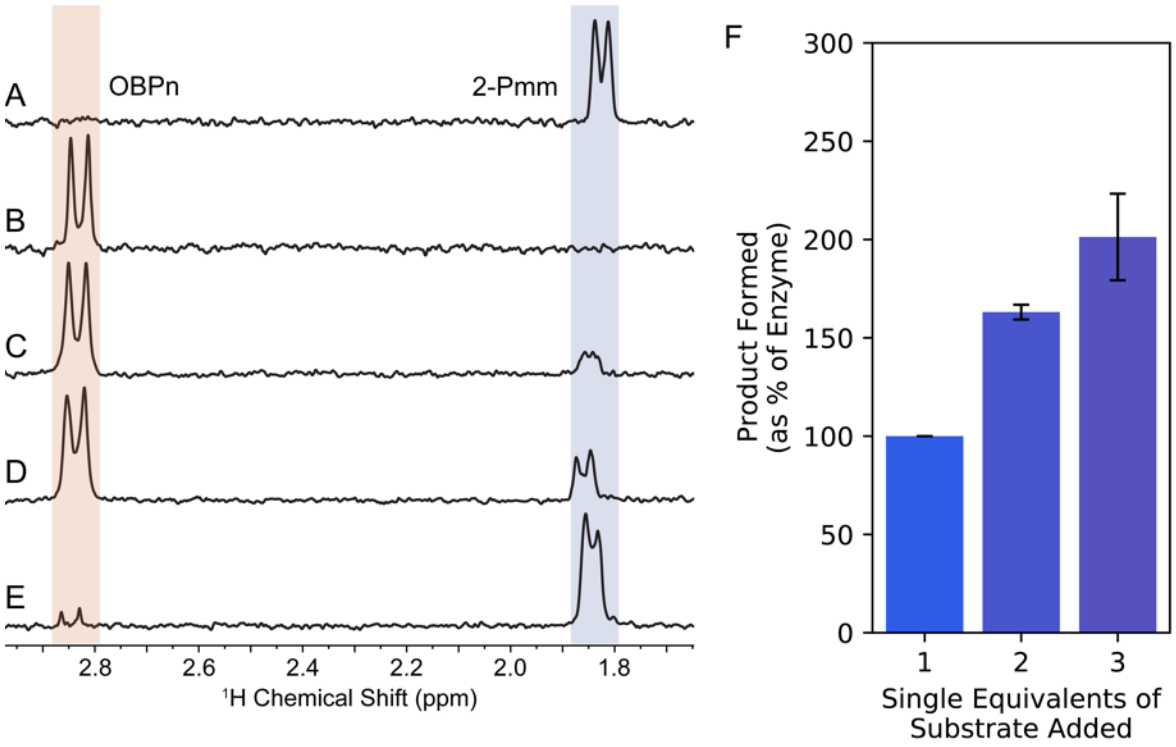

Figure S12. ^{1}H NMR spectra of the upfield region of the products of single-turnover assays of Fe-reconstituted PsfC. 2-Pmm was assayed with Fe-reconstituted and twice-dialyzed PsfC under aerobic conditions. Reactions were quenched 30 s after addition of substrate by addition of EDTA to 15 mM. A) Control reaction showing that 100 μM 2-Pmm (~1.8 ppm) added to dialysis buffer (containing non-protein-bound Fe) shows no product formation. B) Reaction of 100 μM 2-Pmm with 100 μM Fe-reconstituted PsfC shows complete turnover to 3-OBPn (~2.9 ppm). C) An additional equivalent of 2-Pmm (total 200 μM) was added 30 s after taking the spectrum of the sample in **B**. D) A third equivalent of 2-Pmm (100 μM, total 300 μM) was added to the sample in panel **C**. E) Reaction performed as in **B** but with 200 μM 2-Pmm added as single addition to PsfC shows less turnover than two consecutive single-turnover reactions with 100 μM (reaction **C**). Data shown are ^{1}H projections of ^{1}H-^{31}P HMBC spectra recorded as described in *Materials and Methods*. F) Product formed in **B-D** as proportion of substrate added indicates PsfC can perform multiple turnovers when substrate 2-Pmm is not in excess over enzyme.

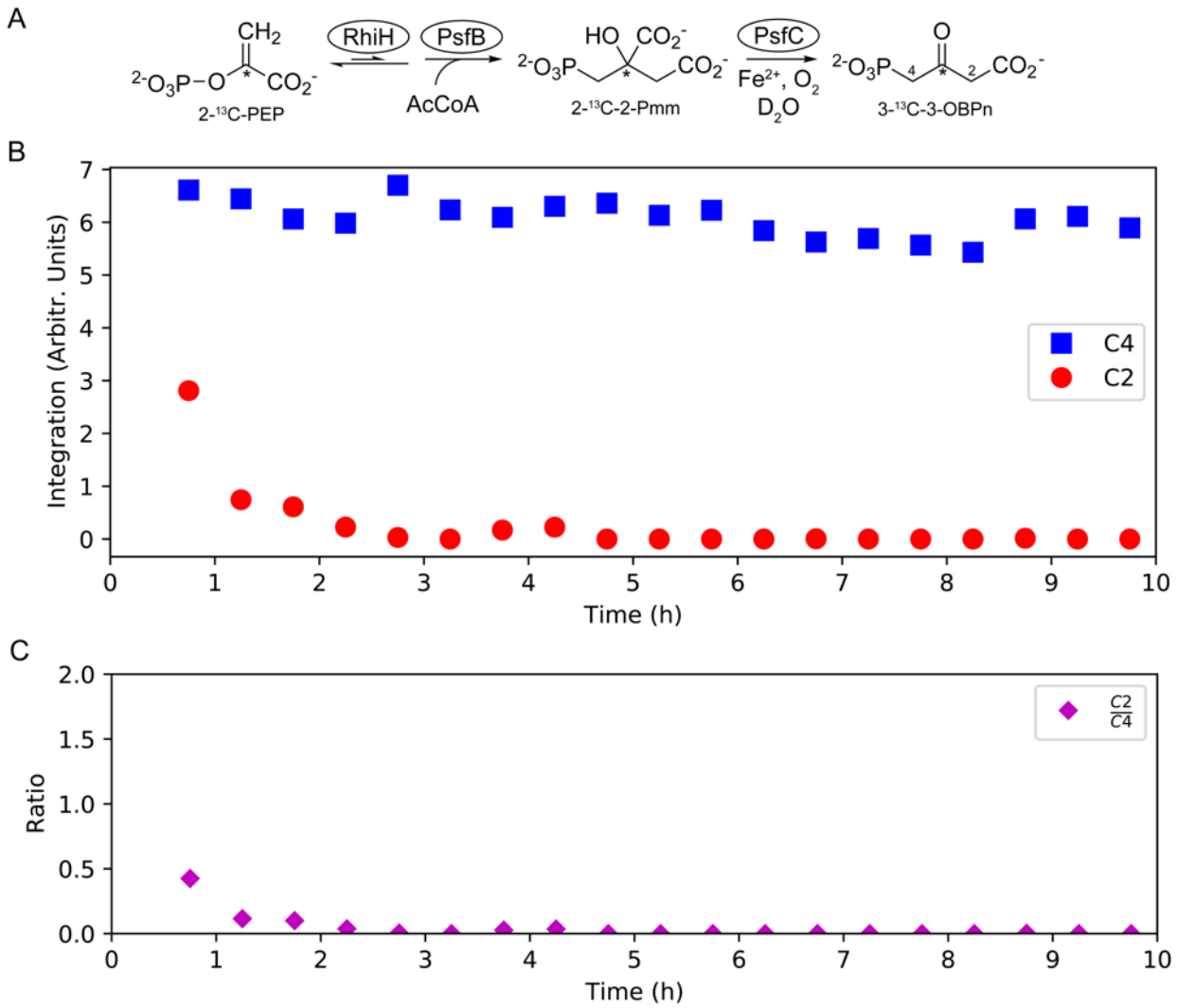

Figure S13. Probe of hydrogen-deuterium solvent exchange at C2 and C4 of 3-OBPn. A) 3-^{13}C-3-OBPn was produced enzymatically, and B) the product was monitored over time by ^{1}H-^{13}C gHMBCAD. Integrations of peaks corresponding to protons at C2 (red) and C4 (blue) of 3-^{13}C-3-OBPn dissolved in D_2O were averaged over three experiments and plotted over time. The intensity of the signal corresponding to the protons at C2 decreases as a result of exchange with deuterium from solvent. The intensity of the signal from the protons at C4 does not change over time indicating they do not exchange with solvent. C) The corresponding ratio of C2/C4 decreases to 0 after 1-2 hours of incubation in D_2O.

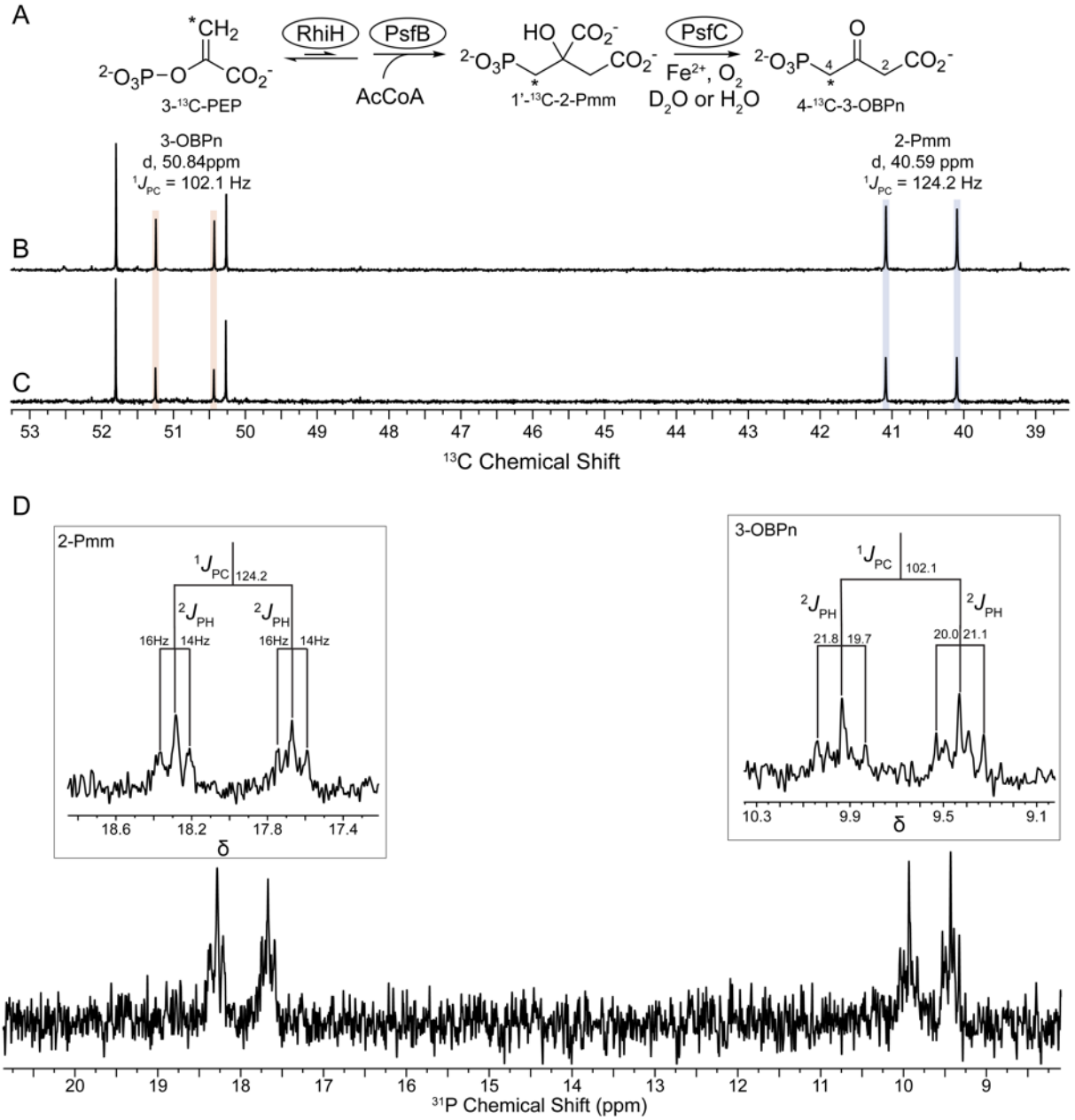

Figure S14. 1D-^{13}C and ^{31}P NMR spectra of 3-OBPn product generated by PsfC in D_2O and in H_2O. A) 4-^{13}C-3-OBPn was produced by PsfC in H_2O or 80% D_2O and monitored by ^{1}H-decoupled ^{13}C NMR; no difference was observed for reactions performed in (**B**) H_2O or (**C**) D_2O (80%). (**D**) ^{1}H-coupled ^{31}P NMR spectrum of the sample in **C** illustrates both 2-Pmm (inset left) and 3-OBPn (inset right) appear as a doublet of triplets, suggesting no deuterium substitution in the product at C4.

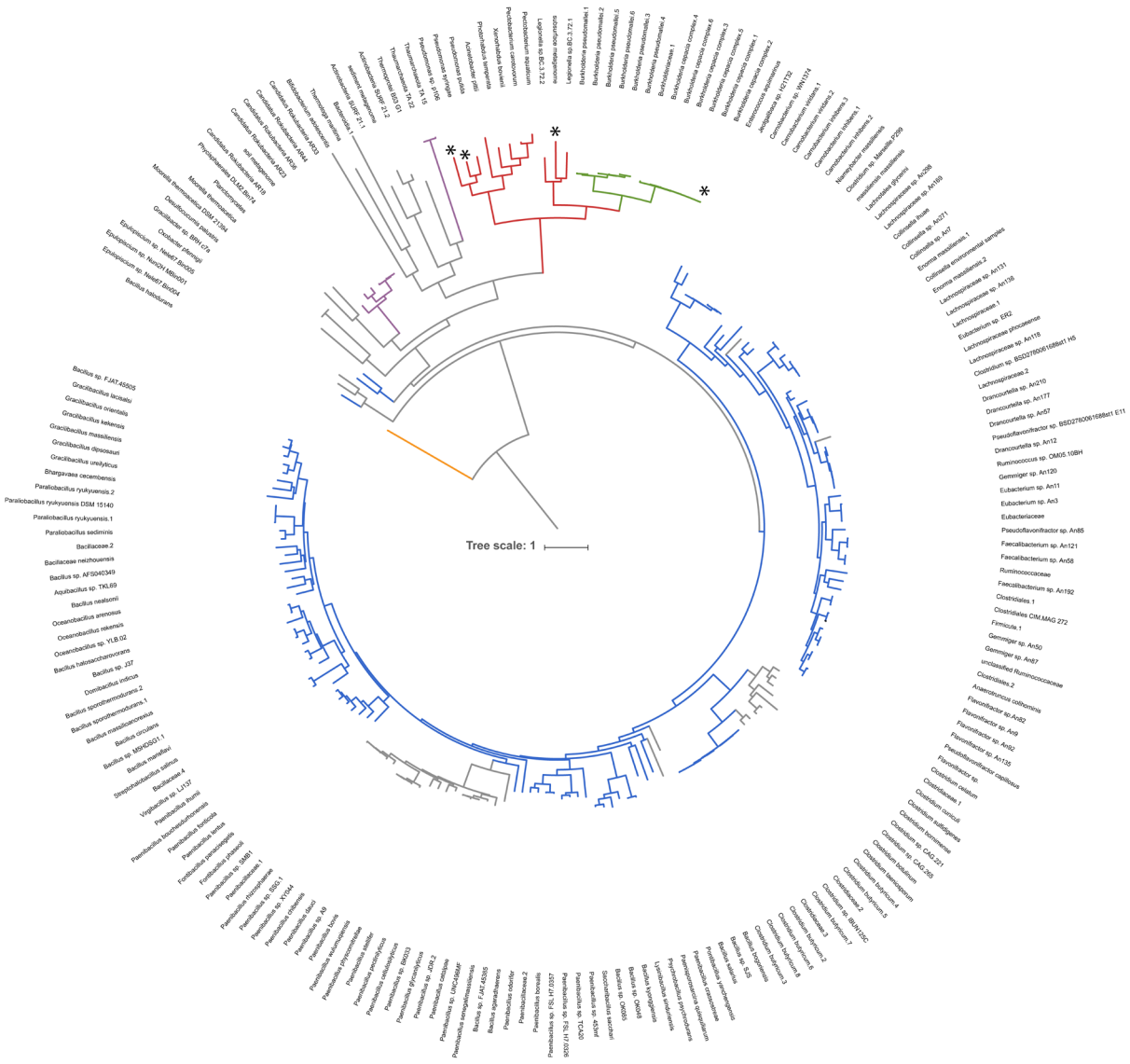

Figure S15. Phylogenetic analysis of PsfC. Accession numbers with organism names are listed in Table S2. Functionally verified members are denoted with an asterisk (*).

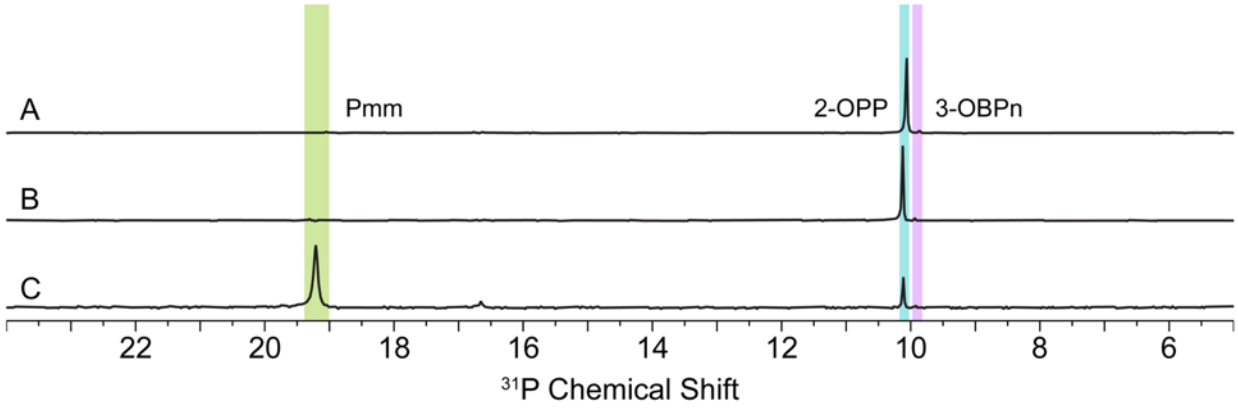

Figure S16. Co-expression of PsfC homologs produce the same products as PsfC from the fosfomycin pathway. Homologs from three organisms identified in the phylogenetic analysis of PsfC were individually co-expressed with *psfAB* from *P. syringae* PB-5123. All three produced 2-OPP and 3-OBPn, verified by ^{1}H-^{31}P HMBC. ^{31}P spectra were recorded after co-expression of *psfAB* with *psfC*-homologs from A) *Pseudomonas* sp. p106 (*Ps106*PsfC, WP_125924462.1), B) *Burkholderia stagnalis* (*Bs*PsfC, WP_059908919.1), and C) *Gammaproteobacterium bacteria* (*Gb*PsfC, OGT51126.1). ^{31}P chemical shifts of phosphonates are sensitive to pH near their pK_a resulting in small shifts from experiment to experiment. Under the work-up conditions used, 3-OBPn converts to 2-OPP.

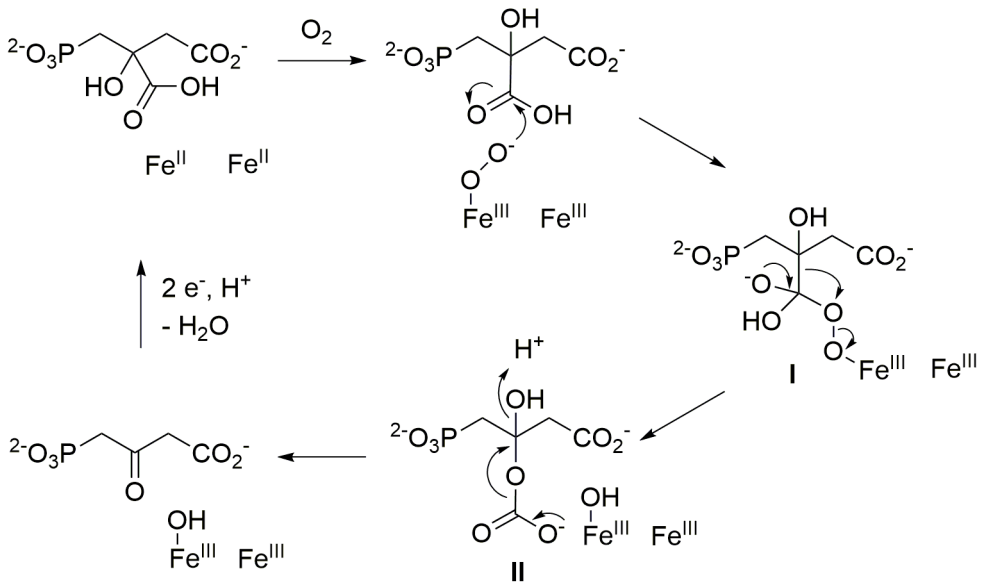

Scheme S1. An alternative mechanism of oxidative decarboxylation. As discussed in the main text, the mechanisms in Scheme 1 infer hydrogen atom transfer (HAT) from C2 because NMR data argue against abstraction from C4. However, direct experimental evidence for HAT from C2 could not be obtained because the protons at C2 of the product exchange too fast with solvent. As a result, a mechanism that does not involve HAT from either C2 or C4 would also be consistent with the data. One such mechanism is shown here. The two ferrous ions could provide the two required electrons to form a ferric-peroxo, which might attack the carboxylic acid (provided it was protonated or activated in some other fashion). A Criegee-like rearrangement from the tetrahedral intermediate **I** could then break the C-C bond and form carbonate **II**, which could decarboxylate to provide the 3-OBPn product. We are not aware of any precedent for such a mechanism in iron-dependent enzymes but since it would explain the data, it is shown for completeness.

Table S1. Average distances between Fe-Fe for select diiron enzymes.

	PDB ID	Monomer	Fe-Fe (Å)
sMMOH	1MTY	A	3.04
		B	3.14
Oxy-Hemerythrin	1HMO	A	3.27
		B	3.29
		C	3.27
		D	3.26
CmlA	5KIK	A	3.33
AurF	2JCD	A	3.55
		B	3.66
DOHH	4D50	A	3.68
		B	3.77
RNR R2	1XIK	A	3.94
		B	3.88
UndA	6P5Q	A	4.85
		B	4.46
SznF*	6VZY	-	5.00

*SnzF information taken from (16). All other distances were identified using deposited coordinates from the PDB.

Table S2. Accession numbers used for phylogenetic analysis of PsfC (Figure S15). Bolded members were functionally characterized in this study.

Branch label	**Accession Number**
Acinetobacter pittii	WP 087090869.1
Actinobacteria SURF 21.1	RJP34514.1
Actinobacteria SURF 21.2	RJP34515.1
Anaerotruncus colihominis	WP_117546765.1
Aquibacillus sp. TKL69	WP_143891742.1
Aquifex aeolicus	WP_010880626.1
Bacillaceae.1	WP_002011701.1
Bacillaceae.2	WP_112181886.1
Bacillaceae.3	WP_011232273.1
Bacillaceae.4	WP_062321281.1
Bacillaceae neizhouensis	WP_110935369.1
Bacilli.1	WP_003227815.1
Bacilli.2	WP_003229318.1
Bacillus.3	WP_000861818.1
Bacillus agaradhaerens	WP_078576593.1
Bacillus bogoriensis	WP_026672943.1
Bacillus circulans	TRZ39878.1
Bacillus halodurans	WP_010899349.1
Bacillus halosaccharovorans	WP_078431422.1
Bacillus kyonggiensis	WP_136831967.1
Bacillus marisflavi	WP_121618573.1
Bacillus massilioanorexius	WP_019240582.1
Bacillus nealsonii	WP_016200772.1
Bacillus salaries	WP_125560471.1
Bacillus sp. AFS040349	WP_098799700.1
Bacillus sp. FJAT.45385	WP_088104464.1
Bacillus sp. FJAT.45505	WP_100359422.1
Bacillus sp. J37	WP_026559147.1
Bacillus sp. M5HDSG1.1	WP_127739148.1
Bacillus sp. OK048	WP_090761906.1
Bacillus sp. OK085	WP_132096419.1
Bacillus sp. SJS	WP_035413352.1
Bacillus sporothermodurans.1	WP_066232796.1
Bacillus sporothermodurans.2	WP_107920736.1
Bacillus subtilis.1	5J21_A
Bacillus subtilis.2	BAM52305.1
Bacteroidia.1	WP_005842464.1

Bhargavaea cecembensis	WP_063182092.1
Bifidobacterium adolescentis	WP_011743495.1
Brevibacillus brevis	WP_012683809.1
Burkholderia cepacia complex.1	WP_059558875.1
Burkholderia cepacia complex.2	WP_059908919.1
Burkholderia cepacia complex.3	WP_060365175.1
Burkholderia cepacia complex.4	WP_124519125.1
Burkholderia cepacia complex.5	WP_124596460.1
Burkholderia cepacia complex.6	WP_124887051.1
Burkholderia pseudomallei.1	WP_010109219.1
Burkholderia pseudomallei.2	WP_010119098.1
Burkholderia pseudomallei.3	WP_059472090.1
Burkholderia pseudomallei.4	WP_059598516.1
Burkholderia pseudomallei.5	WP_066491349.1
Burkholderia pseudomallei.6	WP_066572434.1
Burkholderiaceae.1	WP_124512156.1
Candidatus Rokubacteria AR18	PYO01206.1
Candidatus Rokubacteria AR23	PYN73540.1
Candidatus Rokubacteria AR33	PYN14251.1
Candidatus Rokubacteria AR36	PYM86219.1
Candidatus Rokubacteria AR44	PYM33524.1
Carnobacterium inhibens.1	AGY82610.1
Carnobacterium inhibens.2	WP_081701929.1
Carnobacterium inhibens.3	WP_081901371.1
Carnobacterium sp. WN1374	WP_081896451.1
Carnobacterium viridans.1	SDQ29467.1
Carnobacterium viridans.2	WP_089977088.1
Chromobacterium violaceum	2YB1_A
Clostridiaceae.1	WP_042393906.1
Clostridiaceae.2	WP_043853810.1
Clostridiaceae.3	WP_070779580.1
Clostridiales.1	WP_089706110.1
Clostridiales.2	WP_110441477.1
Clostridiales CIM.MAG 272	PWM22748.1
Clostridium bornimense	WP_044039469.1
Clostridium botulinum	WP_035782989.1
Clostridium butyricum.1	EDT74077.1
Clostridium butyricum.2	ETI87721.1
Clostridium butyricum.3	GEQ20569.1
Clostridium butyricum.4	WP_002581741.1

Clostridium butyricum.5	WP_003430874.1
Clostridium butyricum.6	WP_027634878.1
Clostridium butyricum.7	WP_035763983.1
Clostridium butyricum.8	WP_124230146.1
Clostridium celatum	WP_005215243.1
Clostridium cuniculi	WP_133016623.1
Clostridium sp. BSD2780061688st1 H5	WP_138302937.1
Clostridium sp. CAG.221	CDB15711.1
Clostridium sp. CAG.265	CDB74890.1
Clostridium sp. IBUN125C	KJZ84038.1
Clostridium sp. Marseille.P299	WP_066717357.1
Clostridium sulfidigenes	WP_035131859.1
Clostridium taeniosporum	WP_069679751.1
Collinsella environmental samples	CDD41077.1
Collinsella ihuae	WP_066831160.1
Collinsella sp. An271	WP_087200767.1
Collinsella sp. An7	WP_087355930.1
Desulfocucumis palustris	WP_104372931.1
Domibacillus indicus	WP_046175969.1
Drancourtella sp. An12	WP_087167055.1
Drancourtella sp. An177	WP_087210278.1
Drancourtella sp. An210	WP_087202035.1
Drancourtella sp. An57	WP_087253610.1
Enorma massiliensis.1	WP_019127859.1
Enorma massiliensis.2	WP_087186749.1
Enterococcus aquimarinus	WP_071874080.1
Epulopiscium sp. Nele67.Bin004	OON99087.1
Epulopiscium sp. Nele67.Bin005	OON96071.1
Epulopiscium sp. Nuni2H MBin001	OOB79275.1
Escherichia coli.1	AKK12342.2
Escherichia coli.2	WP_103809405.1
Eubacteriaceae	WP_090127354.1
Eubacterium sp. An11	WP_140401491.1
Eubacterium sp. An3	WP_087281340.1
Eubacterium sp. ER2	WP_033127123.1
Faecalibacterium sp. An121	WP_087229524.1
Faecalibacterium sp. An192	WP_087365006.1
Faecalibacterium sp. An58	WP_087324950.1
Firmicute.1	CDD27577.1
Flavonifractor sp.	SCI97575.1

Flavonifractor sp. An135	WP_087380394.1
Flavonifractor sp. An9	WP_087399922.1
Flavonifractor sp. An92	WP_087262443.1
Flavonifractor sp.An82	WP_087337310.1
Fontibacillus panacisegetis	WP_091234269.1
Fontibacillus phaseoli	WP_114497580.1
Gemmiger sp. An120	WP_087172009.1
Gemmiger sp. An50	WP_087181920.1
Gemmiger sp. An87	WP_087184910.1
Geobacillus thermoleovorans	BAD75543.1
Gracilibacillus dipsosauri	WP_109983033.1
Gracilibacillus kekensis	WP_073199043.1
Gracilibacillus lacisalsi	WP_018930332.1
Gracilibacillus massiliensis	WP_058308351.1
Gracilibacillus orientalis	WP_091480667.1
Gracilibacillus ureilyticus	WP_089743859.1
Gracilibacter sp. BRH c7a	KUO58778.1
Jeotgalibaca sp. H21T32	WP_126108452.1
Lachnospiraceae.1	WP_087269411.1
Lachnospiraceae.2	WP_117468856.1
Lachnospiraceae phocaeense	WP_076779481.1
Lachnospiraceae sp. An118	WP_087175325.1
Lachnospiraceae sp. An131	WP_087165922.1
Lachnospiraceae sp. An138	WP_087306802.1
Lachnospiraceae sp. An169	WP_087159982.1
Lachnospiraceae sp. An298	WP_087151577.1
Lachnotalea glycerini	WP_094375661.1
Lactococcus lactis	WP_003131121.1
Legionella sp.BC.3.72.1	PJD91620.1
Legionella sp.BC.3.72.2	PJD91621.1
Lysinibacillus sinduriensis	WP_036200076.1
Macrococcus caseolyticus	WP_012656252.1
massiliensis massiliensis	WP_054251776.1
Moorella thermoacetica	WP_082297226.1
Moorella thermoacetica DSM 21394	OIQ55514.1
Moraxellaceae	WP_001160984.1
Mycobacterium tuberculosis	AMC68307.1
Mycoplasma pneumoniae	WP_010874497.1
Niameybacter massiliensis	WP_053982924.1
Oceanobacillus arenosus	WP_115774139.1

Oceanobacillus rekensis	WP_087974702.1
Oceanobacillus sp. YLB.02	WP_121523375.1
Oxobacter pfennigii	WP_054877098.1
Paenibacillaceae.1	WP_105444306.1
Paenibacillaceae.2	WP_042234140.1
Paenibacillus borealis	WP_076110148.1
Paenibacillus bouchesdurhonensis	WP_110930267.1
Paenibacillus bovis	WP_060532868.1
Paenibacillus catalpae	WP_091188553.1
Paenibacillus cellulosilyticus	WP_110045449.1
Paenibacillus chibensis	WP_127605437.1
Paenibacillus crassostreae	WP_068660689.1
Paenibacillus dauci	WP_046228258.1
Paenibacillus fonticola	WP_019635325.1
Paenibacillus glycanilyticus	WP_127497391.1
Paenibacillus ihumii	WP_055106647.1
Paenibacillus lentus	WP_125081105.1
Paenibacillus odorifer	WP_076119532.1
Paenibacillus pectinilyticus	WP_065850928.1
Paenibacillus physcomitrellae	WP_094094874.1
Paenibacillus rhizosphaerae	WP_076173828.1
Paenibacillus senegalimassiliensis	WP_059050569.1
Paenibacillus sp. 453mf	WP_091156300.1
Paenibacillus sp. A9	WP_017811744.1
Paenibacillus sp. BK033	WP_132312841.1
Paenibacillus sp. FSL H7.0326	WP_076315224.1
Paenibacillus sp. FSL H7.0357	WP_038593686.1
Paenibacillus sp. JDR.2	WP_012772289.1
Paenibacillus sp. SMB1	WP_111144931.1
Paenibacillus sp. SSG.1	WP_089548747.1
Paenibacillus sp. TCA20	GAK40618.1
Paenibacillus sp. UNC496MF	WP_090639842.1
Paenibacillus sp. XY044	WP_094597195.1
Paenibacillus stellifer	WP_038694973.1
Paenibacillus wulumuqiensis	WP_046216001.1
Paenisporosarcina quisquiliarum	WP_090566887.1
Paraliobacillus ryukyuensis.1	WP_079711015.1
Paraliobacillus ryukyuensis.2	WP_113867764.1
Paraliobacillus ryukyuensis DSM 15140	RBP00764.1
Paraliobacillus sediminis	WP_117168781.1

Pectobacterium aquaticum	WP_116155214.1
Pectobacterium carotovorum	WP_052237778.1
Photorhabdus temperata	WP_051769179.1
Phycisphaerales DLM2.Bin74	TVQ60296.1
Planctomycetes	RMH28972.1
Pontibacillus yanchengensis	WP_084102975.1
Pseudoflavonifractor capillosus	WP_006574578.1
Pseudoflavonifractor sp. An85	WP_087258172.1
Pseudoflavonifractor sp. BSD2780061688st1 E11	WP_138373423.1
Pseudomonas aeruginosa	PTC38341.1
Pseudomonas putida	WP_136914820.1
Pseudomonas sp. p106	WP_125924462.1
Pseudomonas syringae	AFM38988.1
Psychrobacillus psychrodurans	WP_093494959.1
Ruminococcaceae	WP_087247369.1
Ruminococcus sp. OM05.10BH	WP_118636107.1
Saccharibacillus sacchari	WP_037286588.1
sediment metagenome	OFW57282.1
soil metagenome	OLD51090.1
Staphylococcus aureus	P63982.1
Streptococcus mutans.1	WP_002263062.1
Streptococcus mutans.2	WP_002263149.1
Streptococcus pneumoniae	WP_000565352.1
Streptococcus pyogenes	WP_011285191.1
Streptohalobacillus salinus	WP_110251699.1
subsurface metagenome	OGT51126.1
Thaumarchaeota TA 15	TLX87356.1
Thaumarchaeota TA 22	TLX85415.1
Thermoprotei B53 G1	RLE67673.1
Thermotoga maritima	WP_004081319.1
Thermus aquaticus	Q9XDH5.1
Thermus thermophilus.1	WP_011227759.1
Thermus thermophilus.2	WP_011227864.1
unclassified Ruminococcaceae	WP_008982155.1
Virgibacillus sp. LJ137	WP_123317284.1
Xenorhabdus bovienii	WP_046336670.1

Table S3. Oligonucleotides used in this study

Name	5' Sequence 3'
PsfA F	CCATCATCACCACAGCCAGGATCCGAATTCAATGTCATCAATAACGCATGC
PsfA R	TCGACTTAAGCATTATGCGGCCGCAAGCTTTACCGTGCATACAAACGC
PsfB-RSF F	GTTAAGTATAAGAAGGAGATATACATATGGAAGGCGTCATGAATATTC
PsfB-RSF R	AGCGGTGGCAGCAGCCTAGGTTAATTAATCATTTCAGCGTCGCATG
PsfCM2 F	CTGGTGCCGCGCGGCAGCATGAACAGGAAAGTCGTG
PsfCM2 R	CTTTGTTAGCAGCCGGATCCTTAGCCCATCAGTGATTG
PsfC H22A F	GACACGGCGGTTCACTTGTTGTTGAGCAAAAAACAG
PsfC H22A R	GTGAACCGCCGTGTCCACGACTTTCCTGTTCATAATG
PsfC H24A F	CATGTTGCCTTGTTGTTGAGCAAAAAACAGCGCG
PsfC H24A R	CAACAAGGCAACATGCGTGTCCACGACTTTCCTG
PsfC S28A F	GCGCTGTTTTTTGGCCAACAACAAGTGAACATGCGTGTCC
PsfC S28A R	TGTTGTTGGCCAAAAAACAGCGCGTGCCCGATTGGGCGGC
PsfC K29A F	ATGTTCACTTGTTGTTGAGCGCAAAACAGCGCG
PsfC K29A R	GCCCAATCGGGCACGCGCTGTTTTGCGCTCAACAAC
PsfC K30A F	ATGTTCACTTGTTGTTGAGCAAAGCACAGCGCG
PsfC K30A R	GCCCAATCGGGCACGCGCTGTGCTTTGCTCAACAAC
PsfC Q31A F	AAAAAAGCGCGCGTGCCCGATTGGGCGGCGATC
PsfC Q31A R	CACGCGCGCTTTTTTGCTCAACAACAAGTGAAC
PsfC D35A F	CGCGTGCCCGCTTGGGCGGCGATCAAGCGGATGCTCGATGTG
PsfC D35A R	CGCCGCCCAAGCGGGCACGCGCTGTTTTTTGCTCAACAACAAG
PsfC E58A F	ACCGCGCACATCGAGGCCGATGGCTATCAAACCTTG
PsfC E58A R	CTCGATGTGCGCGGTAACGCATAGCGCATCCAGTTCATC
PsfC H59A F	ACCGAGGCGATCGAGGCCGATGGCTATCAAACCTTG
PsfC H59A R	CTCGATCGCCTCGGTAACGCATAGCGCATCCAGTTCATC
PsfC Q91A F	ACTTACGCGGGTGTCGCCATTTTTCCGGGAGCGGAGCTTG
PsfC Q91A R	GACACCCGCGTAAGTGAGCCGCCCAGCGTGCTG
PsfC E100A F	TTTCCGGGAGCGGCGCTTGAGTTGGCCAACAGGACCAACG
PsfC E100A R	CTCAAGCGCCGCTCCCGGAAAAATGGCGACACCCTGGTAA
PsfC H149A F	GTGGCTGCTCACATTTTCTGGCCGGGCAAGACCTG
PsfC H149A R	AATGTGAGCAGCCACCAGCTTGAAAGGCCTGC
PsfC H150A F	GCTCATGCCATTTTCTGGCCGGGCAAGACCTGTGAC
PsfC H150A R	GAAAATGCATGAGCCACCAGCTTGAAAGGCCTGC
PsfC E172A F	GCCATCGCGGTGCCGGCGAAGGACCTGGCAAATG
PsfC E172A R	CGGCACCGCGATGGCGTTCACATAGCGACCCAG
PsfC K176A F	CCGGCGGCGGACCTGGCAAATGCGCAGAATTATGTTG
PsfC K176A R	CAGGTCCGCCGCCGGCACTTCGATGGCGTTCACATAGCGACCCAG
PsfC D200A F	GGCTCCGCGGCGCATACCTTCATTCAGGTGGGGGCCTGC
PsfC D200A R	ATGCGCCGCGGAGCCACCCGTGGTGTCAAG
PsfC H202A F	GATGCGGCGACCTTCATTCAGGTGGGGGCCTGCCGTAC
PsfC H202A R	GAAGGTCGCCGCATCGGAGCCACCCGTGGTGTCAAG
PsfF F	CTGGTGCCGCGCGGCAGCCATATGAAACCGGCCTGCTATG
PsfF R	CTTTGTTAGCAGCCGGATCCTCGAGTCACTCGCTCAAGAACAC
Psf8 F	CTGGTGCCGCGCGGCAGCCATATGCTAATTACGCTTGCCGGTATCGATGGG
Psf8 R	CTTTGTTAGCAGCCGGATCCTCGAGTCATGGGCGCCCCTGCAGCA
Psf10 F	CTGGTGCCGCGCGGCAGCCATATGGCCAACCCTGAAAGC

Psf10 R	TCGGGCTTTGTTAGCAGCCGGATCCTTAGACATGTTCAGGCTCAATC
Psf12 F	GCCGCGCGGCAGCCATATGATGAGTTGCAAGCGGCTG
Psf12 R	GCTTTGTTAGCAGCCGGATCCTCATAATGACCCCATCACTGATG
PsfD Duet F	TAAGAAGGAGATATACATATATGAACCGCGTGGTGGGG
PsfD Duet R	TTTCTTTACCAGACTCGAGGTCATGACGCCTTCCATGCTTTG
PsfE F	AGCTCGGCGCGCCTGCAGGTCGACAAGCTTATGGACGTTCGCACTTTA G
PsfE R	TTTCTGTTCGACTTAAGCATTATGCGGCCGCTCAACCATAATTGATGGC AATG
Psf5 F	GTTAAGTATAAGAAGGAGATATACATATGCCAGACACTTTGATC
Psf5 R	CGCAGCAGCGGTTTCTTTACCAGACTCGAGTCAAGCGTAATCGACTGC
*Ps106*PsfC F	CTGGTGCCGCGCGGCAGCATGAAGCGCACTATTCTTGATGC
*Ps106*PsfC R	CTTTGTTAGCAGCCGGATCCTCGAGTTAAGGCTCGCGACGCTC
*Gb*PsfC F	CTGGTGCCGCGCGGCAGCATGAAGATCGACACTCATAC
*Gb*PsfC R	CTTTGTTAGCAGCCGGATCCTTACGCCAAAAATTCCATAC
*Bs*PsfC F	CTGGTGCCGCGCGGCAGCATGAAACTGGATACGCATGTACAC
*Bs*PsfC R	CTTTGTTAGCAGCCGGATCCTTAGGCAGCGGCCTGTTC

Table S4. Plasmids and microorganisms used in this study.

Strain or plasmid	Relevant characteristics	Source or reference
Escherichia coli NEB5α (plasmid maintenance)	fhuA2 Δ(argF-lacZ)U169 phoA glnV44 Φ80 Δ(lacZ)M15 gyrA96 recA1 relA1 endA1 thi-1 hsdR17	New England BioLabs (Ipswich, MA)
Escherichia coli BL21(DE3) (protein overexpression)	huA2 [lon] ompT gal (λ DE3) [dcm] ΔhsdS λ DE3 = λ sBamHIo ΔEcoRI-B int::(lacI::PlacUV5::T7 gene1) i21 Δnin5	New England BioLabs (Ipswich, MA)
Escherichia coli Rosetta 2(DE3) pLysS (protein overexpression)	F^- *ompT* $hsdS_B$(r_B^- m_B^-) *gal dcm* (DE3) pLysSRARE2 (Cam^R)	EMDMillipore (Darmstadt, Germany)
Pseudomonas syringae PB-5123	Fosfomycin-producing strain used in amplification of *psf* genes	Shionogi Co. Ltd.
pRSFDuet	Kan^R empty expression plasmid	Novagen
pACYCDuet	Cm^R empty expression plasmid	Novagen
pETDuet	Amp^R empty expression plasmid	Novagen
pET15b	Amp^R empty expression plasmid	Novagen
pET15b_psfC	Amp^R expression of PsfC	This study
pET15b_psfCM2	Amp^R expression of PsfC-M2 (N-terminal truncant starting at Met14)	This study
pET15b_psfB	Amp^R expression of PsfB	This study
pRSFDuet_his-psfA	Kan^R expression of PsfA	This study
pRSFDuet_his-psfA_psfB	Kan^R co-expression of PsfA, PsfB	This study
pET28b_RhiH	Kan^R expression of RhiH	Borisova et al. Chem Biol 2010
pETDuet_His-PsfC	Amp^R co-expressions of psfC	This study
pETDuet_His-PsfC_psfD	AmpR co-expressions of psfC and psfD	This study
pET15b_psfF	Amp^R co-expressions of psfF	This study
pET15b_psf8	Amp^R co-expressions of psf8	This study
pET15b_psf10	Amp^R co-expressions of psf10	This study
pET15b_psf12	Amp^R co-expressions of psf12	This study

pACYC_psfE_psf5	Cm^R co-expressions of psfE and psf5	This study
pET15b_psfC-H22A	Amp^R (co-)expressions of psfC-m2 H22A mutant	This study
pET15b_psfC-H24A	Amp^R (co-)expressions of psfC-m2 H24A mutant	This study
pET15b_psfC-S28A	Amp^R (co-)expressions of psfC-m2 S28A mutant	This study
pET15b_psfC-K29A	Amp^R (co-)expressions of psfC-m2 K29A mutant	This study
pET15b_psfC-K30A	Amp^R (co-)expressions of psfC-m2 K30A mutant	This study
pET15b_psfC-Q31A	Amp^R (co-)expressions of psfC-m2 Q31A mutant	This study
pET15b_psfC-D35A	Amp^R (co-)expressions of psfC-m2 D35A mutant	This study
pET15b_psfC-E58A	Amp^R (co-)expressions of psfC-m2 E58A mutant	This study
pET15b_psfC-H59A	Amp^R (co-)expressions of psfC-m2 H59A mutant	This study
pET15b_psfC-Q91A	Amp^R (co-)expressions of psfC-m2 Q91A mutant	This study
pET15b_psfC-E100A	Amp^R (co-)expressions of psfC-m2 E100A mutant	This study
pET15b_psfC-H149A	Amp^R (co-)expressions of psfC-m2 H149A mutant	This study
pET15b_psfC-H150A	Amp^R (co-)expressions of psfC-m2 H150A mutant	This study
pET15b_psfC-E172A	Amp^R (co-)expressions of psfC-m2 E172A mutant	This study
pET15b_psfC-K176A	Amp^R (co-)expressions of psfC-m2 K176A mutant	This study
pET15b_psfC-D200A	Amp^R (co-)expressions of psfC-m2 D200A mutant	This study
pET15b_psfC-H202A	Amp^R (co-)expressions of psfC-m2 H202A mutant	This study
pET15b_*Ps106*PsfC	Amp^R (co-)expressions of PsfC homolog from *Pseudomonas* sp. p106	This study
pET15b_*Gb*PsfC	Amp^R (co-)expressions of PsfC homolog from *Gammaproteobacterium bacteria*	This study
pET15b_*Bs*PsfC	Amp^R (co-)expressions of PsfC homolog from *Burkholderia stagnalis*	This study

Table S5. Data Collection and Refinement Statistics

	Native (diiron form)	Derivative (Pb)	Anomalous
Data collection			
Wavelength (Å)	1.127	0.9464	1.739
Resolution (Å)	1.963	1.59	3.1
Resolution range (Å)[1]	65.5 - 1.96 (1.97 - 1.96)	73.9 - 1.59 (1.62 - 1.59)	66.1 - 3.1 (3.16 - 3.1)
Space group	I 41	I 41	I 41
Unit cell	106.8 106.8 83.0	104.4 104.4 83.5	107.7 107.7 83.5
Total reflections	238,132	828,529	111,620
Unique reflections	30,430	59,568	8,732
Multiplicity	7.8 (6.0)	13.9 (12.2)	12.8 (14.1)
Completeness (%)	91.2 (68.9)	100 (99.9)	99.5 (100)
Mean I/sigma (I)	15.6 (2.3)	24.1 (2.5)	16.6 (2.3)
R-merge[2] (%)	9.0 (91.9)	6.2 (82.1)	12.8 (111)
R-meas (%)	9.6 (100)	6.4 (85.8)	13.3 (115)
CC ½	0.997 (0.752)	0.999 (0.809)	0.999 (0.658)
Refinement			
Resolution (Å)	25.0-1.96		
No. reflections	28,900		
R-work	22.6		
R-free[3]	26.3		
Number of atoms			
Protein	3791		
Metals	4		
Water	119		
Average B-factor			
Macromolecules	43.4		
Metals	36.5		
Solvent	43.3		
RMS (angles)	1.3		
Favored (%)	95		
Allowed (%)	3.2		
Outliers (%)	1.6		
Rotamer outliers (%)	1.9		
Clashscore	8.92		

1. Highest resolution shell is shown in parenthesis.

2. $R_{merge} = \Sigma |(I_i - \langle I_i \rangle| \Sigma I_i$ where I_i = intensity of the *i*th reflection and $\langle I_i \rangle$ = mean intensity.

3. R-factor = $\Sigma(|F_{obs}|-k|F_{calc}|)/\Sigma |F_{obs}|$ and R-free is the R value for a test set of reflections consisting of a random 5% of the diffraction data not used in refinement.

REFERENCES

1. Borisova SA, Circello BT, Zhang JK, van der Donk WA, & Metcalf WW (2010) Biosynthesis of rhizocticins, antifungal phosphonate oligopeptides produced by *Bacillus subtilis* ATCC6633. *Chem. Biol.* 17(1):28-37.
2. Peter DM, Vogeli B, Cortina NS, & Erb TJ (2016) A Chemo-Enzymatic Road Map to the Synthesis of CoA Esters. *Molecules* 21(4):517.
3. Vonrhein C*, et al.* (2011) Data processing and analysis with the autoPROC toolbox. *Acta Crystallogr. D* 67(Pt 4):293-302.
4. McCoy AJ*, et al.* (2007) Phaser crystallographic software. *J. Appl. Crystallogr.* 40(4):658-674.
5. Potterton L*, et al.* (2018) CCP4i2: the new graphical user interface to the CCP4 program suite. *Acta Crystallogr. D* 74(Pt 2):68-84.
6. Langer G, Cohen SX, Lamzin VS, & Perrakis A (2008) Automated macromolecular model building for X-ray crystallography using ARP/wARP version 7. *Nat. Protoc.* 3(7):1171-1179.
7. Murshudov GN*, et al.* (2011) REFMAC5 for the refinement of macromolecular crystal structures. *Acta Crystallogr. D* 67(Pt 4):355-367.
8. Emsley P, Lohkamp B, Scott WG, & Cowtan K (2010) Features and development of Coot. *Acta Crystallogr. D* 66(Pt 4):486-501.
9. Katoh K & Standley DM (2013) MAFFT multiple sequence alignment software version 7: Improvements in performance and usability. *Mol. Biol. Evol* 30(4):772-780.
10. Price MN, Dehal PS, & Arkin AP (2010) FastTree 2 – Approximately Maximum-Likelihood Trees for Large Alignments. *PLOS ONE* 5(3):e9490.
11. Tietz JI*, et al.* (2017) A new genome-mining tool redefines the lasso peptide biosynthetic landscape. *Nat. Chem. Biol.* 13(5):470-478.
12. Kim SY*, et al.* (2012) Different biosynthetic pathways to fosfomycin in *Pseudomonas syringae* and *Streptomyces* species. *Antimicrob. Agents Chemother.* 56(8):4175-4183.
13. Garcia P, Arca P, & Evaristo Suarez J (1995) Product of *fosC*, a gene from *Pseudomonas syringae*, mediates fosfomycin resistance by using ATP as cosubstrate. *Antimicrob. Agents Chemother.* 39(7):1569-1573.
14. Kobayashi S, Kuzuyama T, & Seto H (2000) Characterization of the fomA and fomB gene products from *Streptomyces wedmorensis*, which confer fosfomycin resistance on *Escherichia coli*. *Antimicrob. Agents Chemother.* 44(3):647-650.
15. Kuzuyama T, Kobayashi S, O'Hara K, Hidaka T, & Seto H (1996) Fosfomycin monophosphate and fosfomycin diphosphate, two inactivated fosfomycin derivatives formed by gene products of fomA and fomB from a fosfomycin producing organism *Streptomyces wedmorensis*. *J. Antibiot.* 49(5):502-504.
16. McBride MJ*, et al.* (2021) Structure and assembly of the diiron cofactor in the heme-oxygenase-like domain of the N-nitrosourea-producing enzyme SznF. *Proc. Natl. Acad. Sci. U. S. A.* 118(4).